Insights on the March 1998 eruption at Piton de la Fournaise volcano (La Réunion) from microgravity monitoring

Sylvain Bonvalot, Dominique Remy, Christine Deplus, Michel Diament, Germinal Gabalda

Insights on the March 1998 eruption at Piton de la Fournaise volcano (La Réunion) from microgravity monitoring

Sylvain Bonvalot,[1,2] Dominique Remy,[1,2] Christine Deplus,[3] Michel Diament,[3] and Germinal Gabalda[1]

Received 30 March 2007; revised 16 November 2007; accepted 15 January 2008; published 17 May 2008.

[1] We investigate the temporal gravity changes associated with one of the major recent eruptions at Piton de la Fournaise volcano (March 1998) that occurred after an unusual five-year quiet period and initiated a new eruptive cycle. Repeated microgravity surveys allowed us to measure residual gravity changes up to 100 μGal within the Enclos Fouqué caldera for four months before the start of the eruption. We first analyzed the temporal gravity changes and the height changes, also measured at the gravity benchmarks, on the basis of an intrusive dyke model previously proposed for this eruption from InSAR and tilt data. This analysis reveals that such simple model (finite rectangular shaped tensile dislocation) cannot fit both gravity and geodetic data and leads us to propose a dual source gravity model for this eruption. The gravity data inversion using a genetic algorithm search method allows us to quantify the mass change produced by the intrusive dyke (3.9 to 8.7 $\times$ 10^9kg) and to suggest an additional mass increase at sea level depth (4.6 to 7.2 $\times$ 10^{10}kg). We interpret the latter as the effect of magma ascent into a reservoir that occurred within the four months before the eruption. We suggest that high concentrations of gas content in the magma reservoir account for a higher compressibility of the intruded magma and produce significant mass change with moderate surface deformation. The 1996 seismic crisis, interpreted as an upward migration of magmatic fluids into a reservoir located at sea level, might support such a hypothesis.

Citation: Bonvalot, S., D. Remy, C. Deplus, M. Diament, and G. Gabalda (2008), Insights on the March 1998 eruption at Piton de la Fournaise volcano (La Réunion) from microgravity monitoring, *J. Geophys. Res.*, *113*, B05407, doi:10.1029/2007JB005084.

1. Introduction

[2] During the last decade, our understanding of magmatic fluid migrations associated with the basaltic eruption at Piton de la Fournaise volcano (La Réunion island, Indian Ocean) has significantly increased owing to (1) improvements to both the seismic and ground deformation monitoring networks (GPS, EDM, Tilts) operated by OVPF (Observatoire Volcanologique du Piton de la Fournaise) and IPGP (Institut de Physique du Globe de Paris), which allowed the availability of data more accurate and (2) the use of new satellite SAR interferometry data (ENVISAT). It was thus possible to describe the dynamic processes within the plumbing system of the volcano, associated with the most recent volcanic activity, with a high resolution in time and space [*Cayol and Cornet*, 1998; *Sigmundsson et al.*, 1999; *Aki and Ferrazzini*, 2000; *Battaglia and Bachèlery*, 2003; *Froger et al.*, 2004; *Battaglia et al.*, 2005; *Fukushima et al.*, 2005; *Peltier et al.*, 2005]. Another reason for this progress is obviously the intense volcanic activity observed at Piton de la Fournaise in the last few years, with a rate of one or two eruptions per year, that have been closely monitored. The sequence we consider here started with the March 1998 eruption, which occurred after an unusual 6-year period of rest. Because of its duration (196 days) and the amount of emitted magma (about 60.10^6 m^3) this eruption is considered as the most important eruptive event that has occurred at Piton de la Fournaise volcano in the last century. Various seismological and ground deformation studies have recently contributed to the description of the magmatic processes that took then place within the plumbing system of the volcano.

[3] Associated mass redistribution can be assessed for this eruption using discrete and continuous microgravity data acquired at Piton de la Fournaise volcano. In this paper, we present and model the temporal gravity observations encompassing the March 1998 eruption, we also analyze the sensitivity of the gravity model to the data accuracy and to the inversion process with the aim of providing a relevant estimation of source parameters for a mass influx related to a dyke intrusion. We discuss our results in terms of agreement and discrepancies between the ground deformation and gravity data derived models and in terms of magma movements in the initial stages of the 1998 eruption on the basis of a possible contribution of shallow and deep sources.

[1] Institut de Recherche pour le Développement, LMTG (Université de Toulouse-CNRS-IRD-OMP), Toulouse, France.
[2] Formerly at Institut de Physique du Globe de Paris, CNRS, Paris, France.
[3] Institut de Physique du Globe de Paris, CNRS, Paris, France.

0148-0227/08/2007JB005084$09.00

Finally, we discuss how to improve the microgravity monitoring at Piton de la Fournaise for a better understanding of volcano dynamics.

1.1. Background

[4] Piton de la Fournaise volcano (21°07′S – 55°32′E) is located on La Réunion Island, a large intraplate volcanic system in the Indian Ocean. La Réunion is considered as the active expression of a mantle plume or hot spot which can be traced back to the emission of the Deccan Traps, 65 million years ago [*Courtillot et al.*, 1986; *Duccan et al.*, 1989]. The Island is composed on its western half by the dormant and deeply eroded Piton des Neiges volcano (3609 m a.s.l.) and, on its eastern half, by the younger Piton de la Fournaise (hereafter named PDF) volcano (2631 m a.s.l.) which contains a 8 km wide caldera (Enclos Fouqué) open to the sea and formed about 4200 years ago (Figure 1) [*Bachèlery*, 1981; *Lenat and Bachèlery*, 1990; *Abchir*, 1996]. PDF volcano is known to be one of the most active basaltic volcanoes in the world with a predominant effusive activity and a mean rate of two eruptions per year. Most of them take place within the Enclos Fouqué caldera, hosting the presently active central cone (topped by the Dolomieu and Bory craters) or along arcuate NE-SE fracture zones (rift zones). After an unusual period of rest from late 1992 to early 1998, PDF volcano entered in a new sequence of eruptions initiated by the March 9, 1998 eruption. Since this major event, the volcano returned to its more typical eruptive pattern with several short eruptions per year, up to the last huge eruption of April 2007 that led to the collapse of the whole Dolomieu crater.

1.2. The March 1998 Eruption: Constraints From Seismological and Geodetic Data

[5] The eruption started at 1105 UT on March 9 from a segmented 1.5-km-long fissure opened on the northern flank (2450-m high) of the active cone [*Global Volcanism Program (GVP)*, 1998a; *Evans and Staudacher*, 2001]. It produced lava fountains that reached up 50 m high. In the following days, two small scoria cones (Piton Kapor and crater M. and K. Kraft) opened at lower altitudes. On March 11, another vent opened WSW of the summit area and formed an isolated cone (crater F. Hudson). This activity stopped on March 31. The lava effusion started from the main north eruptive vent and fed, during the following months, a voluminous and persistent flow which progressively moved to the East of Enclos Fouqué caldera down to the Indian Ocean (see *GVP* [1998a, 1998b, 1998c, 1998d, 1998e] for more detailed information).

[6] The migration of magmatic fluids in the early stages of this eruption is well documented thanks to the seismological and ground deformation data from the monitoring networks of the Volcanological Observatory of PDF volcano [*GVP*, 1998a, 1998b; *Aki and Ferrazzini*, 2000; *Battaglia and Bachèlery*, 2003]. The seismicity started to increase in early 1998 and turned into a continuous seismic swarm (30 earthquakes per hour) in the hours preceding the eruption. The precursory swarm of volcano-tectonic events started about 5 km below sea level (b.s.l) and beneath the central cone, on March 8 (at 0 UT). The depth of the hypocenters of these events then migrated upward from 5 km to about 2 km b.s.l. In the hour before magma venting, a ground inflation of the summit area associated with a dyke injection to the surface was detected from the continuous ground deformation networks.

[7] The surface deformation produced by the eruptive fissure and its feeder dyke was also observed for the first time at PDF volcano from SAR interferometry data. *Sigmundsson et al.* [1999] produced a series of Radarsat interferograms spanning from 29 May 1996 to 12 June 1998 covering the preeruptive and coeruptive phases. A 576-day-long interferogram including the first two months of the eruption (20 October 1996 to 19 May 1998) clearly shows a surface displacement of 48 cm toward the satellite. This inflation signal shows an asymmetric pattern in which all fringes occur east of the eruptive fissure (seaward) and practically no range change is observed on the western side of the fissure. The resulting deformation corresponds to a seaward displacement and bulging of the active cone. The same pattern was observed for other PDF eruptions. It reflects the structural behavior and the development of the Enclos Fouqué caldera formed by seaward collapses resulting from numerous intrusions and gravitational instability [*Lenat and Bachèlery*, 1990].

[8] The observations provided by both the monitoring networks and spaceborne radar interferometry led to a geodetic model for the March 1998 dyke intrusion based on elastic dislocation modeling [*Sigmundsson et al.*, 1999; *Battaglia and Bachèlery*, 2003]. We will further discuss these results in light of the information provided by our microgravity data.

2. Microgravity Data Acquisition and Processing

2.1. Field Surveys

[9] The microgravity data presented in this study were acquired through repeated field surveys carried out at PDF, jointly by Institut de Physique du Globe de Paris (IPGP) and Institut de Recherche pour le Développement (IRD). This network – that includes an older microgravity and leveling profile established in the early eighties – was designed and measured between 1992 and 1995 [*Bonvalot et al.*, 1996, 1998a, 2003]. The two field surveys encompassing the 1998 eruption were carried out in November 1997 (14 November to 2 December 1997) and March 1998 (11–17 March 1998), respectively. The first one was carried out at the end of the five year period of volcanic rest which followed the last cycle of activity (which ended in July 1992). The second one was accomplished during the initial stage of the 1998 eruption, a week after the opening of the first fissure. The surveyed area includes several profiles distributed inside the Enclos Fouqué caldera (elevations between 2000 and 2600 m). It covers the central active cone and their summit Dolomieu and Bory craters and a series of remote reference stations located outside of the Enclos Fouqué caldera and along the access road to the Volcanological Observatory of Piton de la Fournaise (OVPF) in La Plaine des Caffres (elevation 1500 m) (Figures 1 and 3). Over 40 common stations were measured during both campaigns.

[10] The field surveys were realized according to the data acquisition and processing protocols established for high-precision microgravity monitoring at Piton de la Fournaise [*Bonvalot et al.*, 1996, 1998b; *Gabalda et al.*, 2003]. The

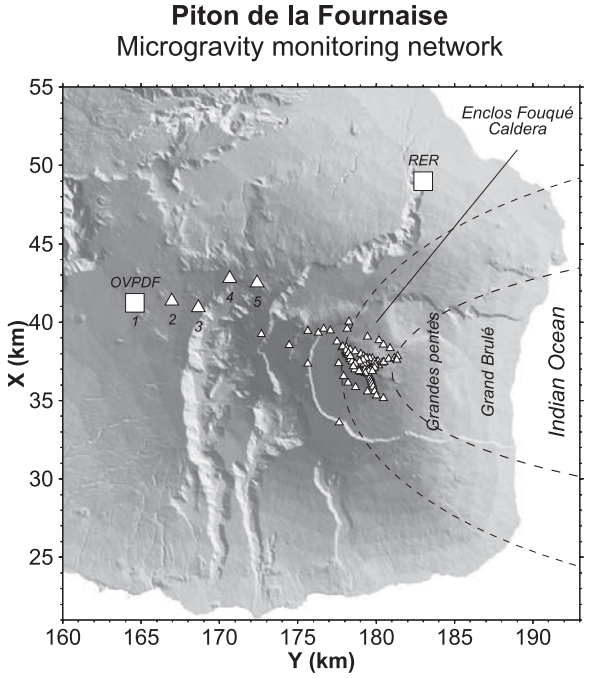

Figure 1. Microgravity monitoring network of Piton de la Fournaise volcano. The small white triangles show the locations of the microgravity stations, and the large triangles show remote stations used to check the instrumental calibration of the gravity meters (with station numbers). The white squares denote the two continuous gravity stations (OVPDF and RER). The topography is the 50-m resolution DEM from IGN (coordinates in kilometers; Gauss-Laborde projection defined for La Réunion). The dashed lines delimitate the arcuate rift zones where most eruptions occur.

gravity measurements were performed using at least two Scintrex CG-3M microgravity meters simultaneously (resolution: 1 μGal = 10^{-8} m.s^{-2}) to ensure redundancy in the gravity observations. The daily gravity surveys were tied to the same reference stations located outside of the active zone and to the remote station at OVPF. Helicopters were occasionally used for transportation between the caldera rim and summit craters or remote areas when starting some of the gravity surveys to reduce closure time of the gravity loops. Differential GPS measurements (using dual-frequency GPS receivers) were also performed during each gravity survey to get relative positioning of the gravity benchmarks with a few centimeters accuracy. Stop-and-go measurements from close reference stations (usually less than 5 km away) were used for this purpose.

2.2. Data Reduction

[11] Although the Scintrex CG-3M instruments may provide real time data processing including Earth tide or instrumental drift corrections, these online corrections are not accurate enough for microgravity studies [*Bonvalot et al.*, 1998b; *Jousset et al.*, 2000; *Gabalda et al.*, 2003]. To achieve a better accuracy in our data reduction, we post-processed the data according to the requirements of high-resolution surveys [*Torge*, 1989; *Seigel et al.*, 1993]. The gravity corrections were computed up to the microGal level using the CG3TOOL package software designed for the processing of Scintrex microgravity data [*Gabalda et al.*, 2003]. The first data reduction step includes precise Earth tide correction, atmospheric corrections and height corrections for the instrumental leveling position at each measurement site. The Earth tide correction was computed using the MT80 prediction software and local tidal model parameters (resulting from the analysis of continuous gravity time series previously acquired at PDF volcano) established by the Royal Observatory of Belgium. The resulting observations acquired with at least two instruments for a given survey were then adjusted using a least squares network procedure resolving simultaneously the calibration factor between instruments and the instrumental drifts. The resulting root mean square (RMS) errors of the network adjustment for the November 1997 and the March 1998 surveys are 5 and 4 μGal, respectively yielding errors of 10 and 8 μGal at the 95% confidence level. Accordingly the error on the temporal gravity change is 13 μGal (95% confidence level).

2.3. Instrumental Calibration and Accuracy of Differential Gravity

[12] As the accuracy of differential gravity data taken at distinct periods with relative instruments depends highly on the stability of the instrumental calibration in time, we took special care to check the instrumental stability of the Scintrex gravity meters we used. The meter calibration was periodically checked and adjusted on absolute gravity stations in France. We also established a reference calibration line on La Réunion Island in a presumed stable area using simultaneously up to four Scintrex CG-3M instruments (see location on Figure 1). The absence of any ground deformation (and thus vertical motions) along this line is attested by more than 20 years of repeated precise leveling or GPS measurements carried out on these stations from the Enclos Fouqué rim up to the Volcanological Observatory (see *Delorme* [1994] and reports of OVPF/IPGP). Assuming that no significant gravity change occurred on these reference stations, we thus adjusted the calibration factors for each instrument by minimizing the discrepancies observed along this line between the measured values (measurements corrected as described in the previous section) and the reference gravity values. We show in Figure 2 the resulting discrepancies observed for the November 1997 and March 1998 surveys with the various Scintrex meters used in this study. It is noteworthy that they mostly remain within 10 μGal over a measurement range of 160 mGal confirming that the instrumental calibration is achieved at both epochs with a relative accuracy better than 10^{-5} as expected for the objective of this study.

2.4. Net Gravity Changes Associated With the 1998 Eruption

[13] Significant ground deformations (pluri-decimetric) accompanied the dyke opening on March 9, 1998 in the surveyed summit area, as revealed by both monitoring network and INSAR data [*GVP*, 1998b; *Sigmundsson et al.*, 1999]. Height changes (uplifts up to 23 cm) at the gravity benchmarks were observed from the GPS measurements carried out simultaneously with the gravity surveys (Table 1). In order to retrieve the net gravity changes, we

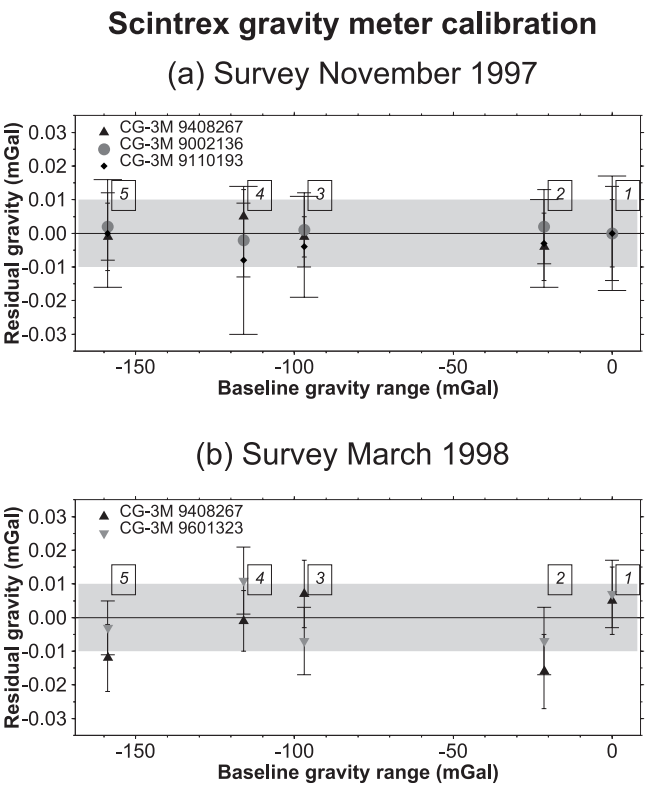

Figure 2. Results of the instrumental calibration of the four Scintrex CG-3M performed on the calibration line at La Réunion in (a) November 1997 and (b) March 1998. The numbers indicate the calibration stations used for meter calibration as shown in Figure 1. The plots show the residual discrepancies between the reference values and the corrected and adjusted gravity observed at each station for the November 1997 and March 1998 surveys. The instrumental calibration is achieved for each epoch with an accuracy better than 10 μGal over a complete measurement range of 160 mGal. The shaded area indicates the 10-μGal interval.

thus removed the gravity effect corresponding to these height changes from our temporal gravity observations. For that, we applied a spherical Bouguer Corrected Free Air Gradient (BCFAG), using the vertical displacement measured by GPS at each gravity station. Following [*Berrino*, 2000; *William-Jones and Rymer*, 2002] the spherical BCFAG correction is expressed in μGal/m as (1):

$$\mathrm{BCFAGspherical} = FAG + \frac{4\pi G \times 10^8}{3}\rho \qquad (1)$$

with *FAG*, the gravity Free Air Gradient (in μGal/m), G the Universal Gravitational constant ($6.67.10^{-11}$ N.m^{2}kg^{-2}) and ρ the mean density of the topography change. According to the uncertainty on the height change (estimated to 30 mm), this height correction will add an additional error of 7 μGal in the height corrected differential gravity signal. The final accuracy of our temporal gravity variations is thus $\sqrt{13^2 + 7^2} \approx 15$ μGal. This value is consistent with those determined for other microgravity networks on active volcanoes [*Rymer*, 1994; *Jousset et al.*, 1995; *Budetta and Carbone*, 1997].

[14] We report in Table 1 our gravity observations. It includes the station coordinates, the observed gravity change, the vertical GPS displacement observed from November 1997 to March 1998, and the corresponding corrected gravity change. The latter was computed using the BCFAG and an arbitrary fixed density value of 2300 kg.m^{-3}, supposed to well approximate the surface density of the uppermost volcanic structure [*Rousset et al.*, 1989; *Deplus et al.*, 1996].

[15] Figure 3 shows the map of the net gravity change resulting from our observations. It displays a NNE-SSW trending signal with maximum amplitude up to 100 μGal (significantly larger than the gravity data accuracy) above the central cone and parallel to the eruptive fissures opened during the first stage of the March 1998 eruption. This short-wavelength signal is superimposed on a longer-wavelength one that exhibits an asymmetric shape with steeper gradients on its western part and gravity values of about 40 to 60 μGal eastward. This map clearly reveals that a significant mass increase occurred in the vicinity of the eruptive fissures during the period covered by our observations. It can be also noted that the largest gravity variations (over 60 μGal) are observed eastward of the eruptive fissure in the area most affected by ground deformations (see Figure 6).

[16] In a first-order approximation, we estimate the net mass influx ΔM detected in the Enclos Fouqué caldera through the Gauss theorem by integrating the observed gravity signal (Δg) over the area (S):

$$\Delta M = \frac{1}{2\pi G}\int\int_S \Delta g dS. \qquad (2)$$

We obtain a mass increase of about 5.4×10^{10} kg for the survey period (November 1997 and March 1998). Obviously, owing to the limited extent of the network in the summit area and to the poorly constrained contoured area (essentially owing to the lack of microgravity observations in the eastern part toward the Grand Brulé), this estimation is only an approximation but probably reflects a lower bound of the true value.

2.5. Complementary Temporal Gravity Observations

[17] Continuous measurements of the gravity field in the vicinity of PDF volcano are also available for the same period. In the few months preceding the March 1998 eruption, we conducted a first experiment of differential gravity monitoring using a pair of Scintrex CG-3M microgravity meters [*Bonvalot et al.*, 1998a]. The operating instruments were set up few km away from the central active cone (outside of Enclos Fouqué caldera and rift zones) to characterize the instrument response and the possible site effects at two reference stations in presumed stable areas (see location in Figure 1): the Volcanological Observatory (OVPF) located at Plaine des Caffres (also used as the reference site for the repeated measurements) and a deep tunnel north of the Enclos Fouqué caldera (RER station also used for a broadband seismic station of the worldwide GEOSCOPE network). Both sites were located inside buildings on concrete pillars. Simultaneous meteorological recordings were also carried out to correct the continuous gravity measurements from external pressure

Table 1. Temporal Gravity and Vertical GPS Changes Measured Between November 1997 and March 1998 at Piton de la Fournaise[a]

Station	X, km	Y, km	ALT, m	ΔG_{RAW}, mGal	Error, mGal	ΔG_{COR}, mGal	ΔZ_{GPS}, m
11	177.151	39.460	2209.86	0.019	0.006	0.019	0.00
16	178.108	38.395	2288.01	0.041	0.008	0.034	−0.03
18	178.654	38.161	2405.72	0.067	0.007	0.067	0.00
19	179.034	37.987	2476.83	0.064	0.008	0.086	0.09
34	179.461	37.685	2519.66	0.004	0.007	0.060	0.23
120	176.664	39.590	2351.73	0.005	0.007	0.003	−0.01
42	177.640	33.590	2274.47	0.012	0.009	0.019	0.03
220	177.875	38.462	2257.00	0.060	0.007	0.048	−0.05
230	178.054	38.205	2310.00	0.051	0.008	0.041	−0.04
240	178.228	38.028	2370.00	0.052	0.008	0.040	−0.05
250	178.341	37.818	2449.00	0.067	0.007	0.067	0.00
260	178.666	37.362	2540.00	0.083	0.008	0.083	0.00
350	178.538	36.835	2522.10	0.066	0.008	0.078	0.05
355	178.448	36.693	2463.20	0.049	0.008	0.061	0.05
365	178.345	36.500	2371.90	0.043	0.008	0.053	0.04
730	178.137	35.860	2208.00	0.002	0.007	0.012	0.04
750	177.607	37.391	2293.00	0.025	0.007	0.027	0.01
600	178.164	39.576	2180.00	0.026	0.007	0.026	0.00
610	179.454	39.072	2157.00	0.078	0.008	0.129	0.21
620	180.184	38.845	2099.00	0.016	0.008	0.055	0.16
630	180.461	38.570	2065.60	0.026	0.008	0.048	0.09
640	180.891	38.313	1980.00	0.053	0.008	0.060	0.03
660	181.321	37.614	1940.60	0.046	0.009	0.046	0.00
555	178.622	36.988	2572.00	0.069	0.006	0.074	0.02
559	179.295	36.764	2514.00	0.060	0.008	0.075	0.06
560	179.028	36.823	2538.00	0.058	0.008	0.063	0.02
562	179.910	37.061	2470.00	0.056	0.008	0.076	0.08
563	179.761	36.879	2487.00	0.067	0.008	0.089	0.09
564	178.552	37.170	2594.70	0.076	0.008	0.083	0.03

[a]The gravity differences are given with respect to reference station Volcanological Observatory of Piton de la Fournaise. ΔG_{raw} and ΔG_{corr} denote the raw temporal gravity changes and the corrected temporal gravity changes, respectively, after applying the height change correction using the spherical BCFAG gradient, the vertical displacement measured at each gravity stations (ΔZ_{GPS}), and a surface density of 2300 kg.m^{-3}. Geographic coordinates are given in Gauss Laborde projection currently used for La Réunion (projection used for all maps in this study).

and temperature effects. Both instruments were setup in early December 1997, but owing to the stabilization time of the gravity meters and to technical problems causing gap in the data series, the differential gravity monitoring really started on February 1998. We report in Figures 4a and 4b the gravity time series recorded at both sites between 19 February 1998 and 16 March 1998 and the computed differential gravity recording encompassing the beginning of the eruption (Figure 4c). First, it is stated that the remoteness of these stations cannot allow us to detect any subsurface processes that occurred in the active zone (dyke intrusion for instance). Nevertheless, these stations could have recorded the consequence of large mass changes below PDF volcano if they are large enough to rise up above the differential measurement accuracy (estimated from this study to about 15 μGal). As shown in Figure 4c, the differential recording displays a quite flat residual signal with little variation remaining within the data accuracy. It is noticeable that the time series are affected by an important noise coinciding with the high standard error values. This high level of noise has been related to tropical low atmospheric pressure front waves that have affected the island and that might have produced local changes in the vicinity of the gravity stations. These observations confirm that no significant temporal gravity variation occurred between those two stations over period of a few days in the few weeks preceding the eruption. It should be noted also that a gravity change that would occur over a period comparable (or longer) than the length of the sequences, would have been compensated by the instrumental drift correction. These results will be discussed later.

3. Modeling Strategies

[18] Using respectively Insar and tilt data, *Sigmundsson et al.* [1999] and *Battaglia and Bachèlery* [2003] showed that the deformation field produced by the dyke intrusion can be explained at first order in terms of a tensile dislocation in a uniform elastic half-space. Their model, based on an *Okada* [1985, 1992] formulation, involves a single source modeled as an inclined rectangular shaped dyke. The model geometry and the resulting model parameters deduced from these studies are given in Figure 5 and Table 2, respectively.

[19] Here, the availability of microgravity and GPS data for this event makes it possible to model both mass transfers and ground deformation related with an eruption fissure. Such a coupled modeling, as proposed by *Okubo and Wanatabe* [1989], allows us to better estimate the source mechanisms associated with a dyke intrusion, as shown for instance in the work of *Jousset et al.* [2003] and *Carbone et al.* [2007]. Following a similar approach, we thus model our data with the aim of evaluating how these observations are consistent with the single source model already proposed for this eruption from the available geodetic data (InSAR and tilt).

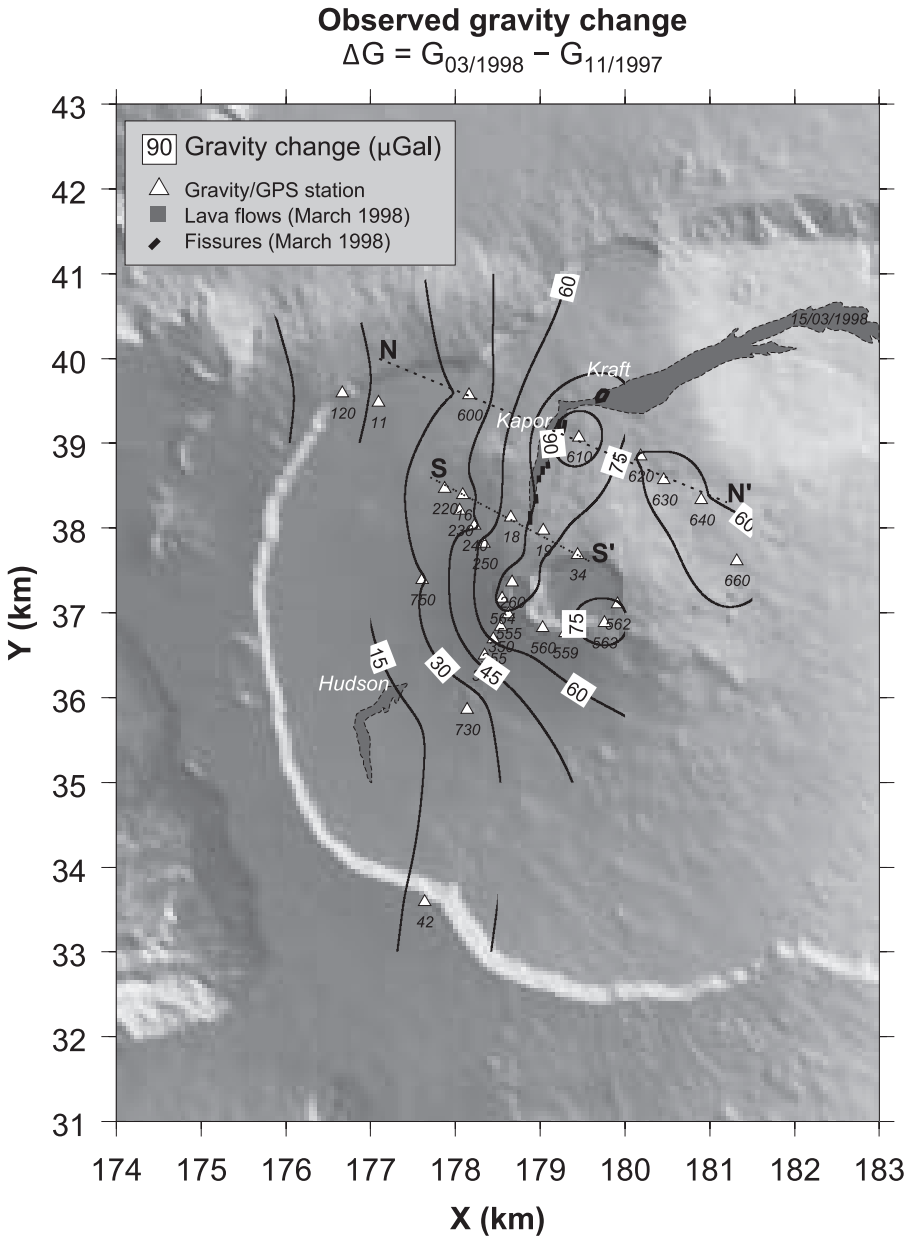

Figure 3. Map of the residual microgravity variations observed in the Enclos Fouqué caldera between November 1997 and March 1998 (isolines in microGal). Residual variations are corrected from height changes measured between the two surveys by GPS measurements. The white triangles with numbers show the location of the microgravity stations as referenced in Table 1. The two profiles NN′ and SS′ used in this study are shown as dashed lines.

3.1. Single Source Model (Superficial Intrusive Dyke)

3.1.1. Coupled Modeling of Gravity and GPS Data (Okubo Model)

[20] We used the analytic approach proposed by *Okubo* [1992] to invert simultaneously the gravity and GPS data. In this formulation, the observed temporal gravity changes and vertical displacements are modeled in terms of a tensile rectangular-shaped dislocation in a uniform elastic half-space. It also allows us to take into account an inclined dyke model as also used for the elastic modeling of ground deformations from InSAR and tilt data. The gravity change caused by the tensile opening is the sum of two contributions, one from the dilatation field and the other from the cavity-filling matter. Both contributions are proportional to the slip vector of the elastic dislocation. It involves 10 parameters: 8 parameters describing the dyke geometry (Figure 5), the density of the host rock (dilatation) and the density of the fresh magma which intrudes into the cavity by tensile fracturing (cavity-filling matter).

[21] The choice of a mean density contrast for fresh magma ascending into the surrounding host rock over the uppermost volcanic structure (down to 1000 m depth) is not straightforward. This parameter is usually poorly constrained as it reflects not only the nature and composition of both ascending magma and the surrounding solidified

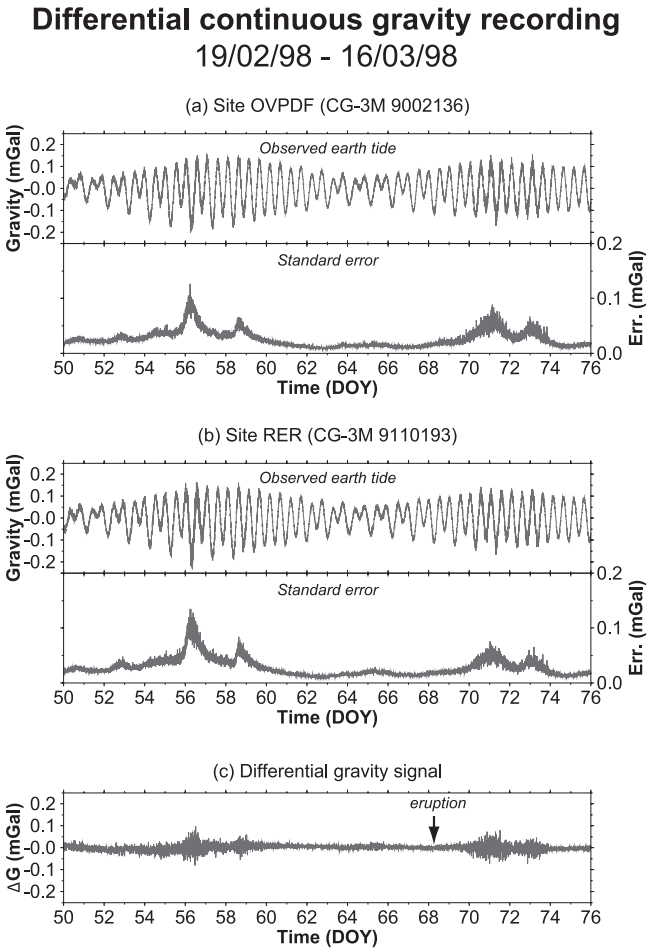

Figure 4. Continuous gravity recordings performed with Scintrex CG-3M meters on remote reference stations at Piton de la Fournaise volcano between 19 February and 16 March 1998. (a and b) The Earth tide recordings (sampling 1 point/min) and the corresponding standard error on the gravity measurements are for sites OVPF and RER, respectively. The time series are corrected for long-term instrumental drift using a linear model. The instrumental drift previously evaluated under laboratory conditions is 0.243 and 0.521 mGal.day^{-1} for meters 9002136 and 9119193, respectively [*Bonvalot et al.*, 1998b]. (c) Differential gravity signal computed as RER-OVPF signals. No evidence of significant gravity change over periods of a few days was observed between these stations before and during the initial stages of the 1998 eruption.

lavas, but also the way in which the magma will fill and close the opened spaces (i.e., porosity of the medium). Typical density values for basaltic compact lavas usually range between 2700 and 3100 kg.m^{-3} [*Villari*, 1969; *William and McBirney*, 1979]. In the case of Piton de la Fournaise, *Lenat and Bachèlery* [1990] showed that the central active cone is essentially composed of a stacking of thin flows, strongly vesiculed and separated by levels of scoria. They also observed, in the wall of the Dolomieu crater, that these flows are cut by numerous void fractures. These observations indicate that the average density of the uppermost structure of PDF is probably lower than these reference values. Results of structural gravity studies also indicate that the central active cone is characterized by relatively low density values (about 2300 kg.m^{-3}; *Rousset et al.* [1989]; *Deplus et al.* [1996]), in agreement with hydrological studies [*Violette*, 1993; *Barcelo*, 1996; *Folio*, 2001; *Join et al.*, 2005]. In the following modeling, we will then assume 800 kg.m^{-3} as the maximum possible density contrast between the host rock and the fresh magma We inverted the data using a genetic algorithm approach (see Appendix A), by searching solutions close to those already proposed by *Sigmundsson et al.* [1999] and *Battaglia and Bachèlery* [2003]. The solutions found reveal that the observed vertical GPS displacements are well fitted by this model, with a RMS error less than 3 cm. Figure 6 shows the observed vectors of displacements and the modeled ones for the best fit model. This result highlights the good consistency of the three data sets (derived from the permanent monitoring network, satellite radar imaging and GPS surveys) that have recorded independently the deformation field for the March 1998 eruption. Logically, as being modeled under the same assumptions of elastic dislocation, the resulting parameters inferred from these data for the dyke geometry are close together (Table 2).

[22] Nonetheless, it should be stressed that the modeled gravity effect found through the inversion process does not match the observed one as indicated by the high RMS error (up to 60 μGal). Figure 7a shows the observed gravity and computed effect using the Okubo model along the two profiles perpendicular to the dyke (profiles named NN' and SS' in Figure 3). This clearly indicates that our temporal gravity observations cannot be explained by this simple source model. As the slip vector in a tensile opening is strongly constrained by the vertical ground displacements, the only way to better mimic the gravity signal is to increase the density for the dyke intrusion. In that case, a density contrast of 16,000 kg.m^{-3} would be required to better reproduce the pattern of the gravity changes and significantly reduces the RMS error by about 50% (30 μGal). A similar result is inferred from the following simple computation considering the dyke geometry inferred from the geodetic data (i.e., InSAR, Tilt and GPS) and the estimation of mass influx deduced from the Gauss approach. Using the dyke parameters given in Table 2, the volume of the dyke model is estimated to range between 1.35 and 3.9 10^6m^3. Then, using the net mass influx ΔM estimated previously, the density contrast between the host rock and the ascending fresh magma would range between 14,000 to 40,000 kg.m^{-3}. These physically unrealistic values suggest that the mass change occurred at PDF volcano cannot be explained by the proposed approach. They lead us to invoke other features to better explain our gravity observations.

3.1.2. Modeling of Gravity Data Using a Meshed Dyke Model (Okabe Model)

[23] The dyke geometry derived from the Okubo approach does not take into account the topography. Using such a simplified geometry may strongly reduce the magnitude of the gravity signal in the near field of the dyke. We thus computed a 3-D gravity model using the *Okabe* [1979] algorithm, which makes it possible to model 3-D sources of any shape. The source dyke model is a finite rectangular prism defined here by nine parameters (the above mentioned 8 parameters describing the dyke geometry and the density contrast). The model is meshed by triangular cells in

Table 2. Parameters of the Dyke Model Deduced From the Okada Modeling of SAR Interferometry (Model "S") and Tilt (Models "B1, B2") Data and From the Coupled Modeling of Gravity and GPS Data ("Okubo" Model)[a]

	X_0, km	Y_0, km	φ, deg	D, m	L, m	W, m	Dip, deg	T, m	Volume, 10^6 m^3
Model S [*Sigmundsson et al.*, 1999]	179.45	37.15	76	744	2500	900	45	0.6	1.35
Model B1 [*Battaglia and Bachèlery*, 2003]	179.16	37.16	83.9	1195.4	2837.1	800.6	57.90	1.64	3.72
Model B2 [*Battaglia and Bachèlery*, 2003]	179.14	37.18	58.9	990.4	2777.4	906.7	55.55	1.11	1.64
Okubo model (this study)	179.42	37.05	73	1200	2960	755	74	1.16	2.59

[a]The meaning of model parameters is reported in Figure 5. A Poisson ration of 0.25 was used for the Okubo modeling.

order to take into account the surface topography. The eruptive fissure system extending from 2450 m to 2100 m in elevation corresponds to the intersection of the dyke with the surface. This enables us to fix the location and the strike angle of the dyke. As the width parameter of the dyke is poorly constrained by the gravity data, we fixed an a priori value of 1000 m according to the geodetic results. The gravity effect generated by the dyke model is computed by summing the contribution of each elementary triangular cell using the *Okabe* [1979] formulation. Our best fit model is obtained with a RMS error of 15 μGal and corresponds to a mass increase of 3.4 10^{10} kg. As shown in Figure 7a, this "Okabe" dyke model better explains the amplitude and the wavelength of the gravity signal in the vicinity of the intrusion (profile NN'), but does not perfectly fit all the observed data. Obviously, density and dyke thickness cannot be solved separately as they are not sensitive parameters in the inversion of gravity data. We assess the minimum dyke thickness by setting the maximum values for both density of the intruding magma (2700 kg.m^{-3}) and porosity of the medium (100%). We obtain a dyke thickness of 4 m which is significantly higher than the values inferred from the geodetic data (see Table 2). In addition, this value is not consistent with geological observations at PDF volcano. *Bachèlery* [1981] showed that most of the old dykes found at the bottom deep eroded cliffs a few kilometers away from the summit have less than one meter of thickness. Furthermore, no previous studies mentioned mechanisms able to produce pluri-metric void fracture systems in which magma may intrude as the ones observed for instance at Etna [*Branca et al.*, 2003].

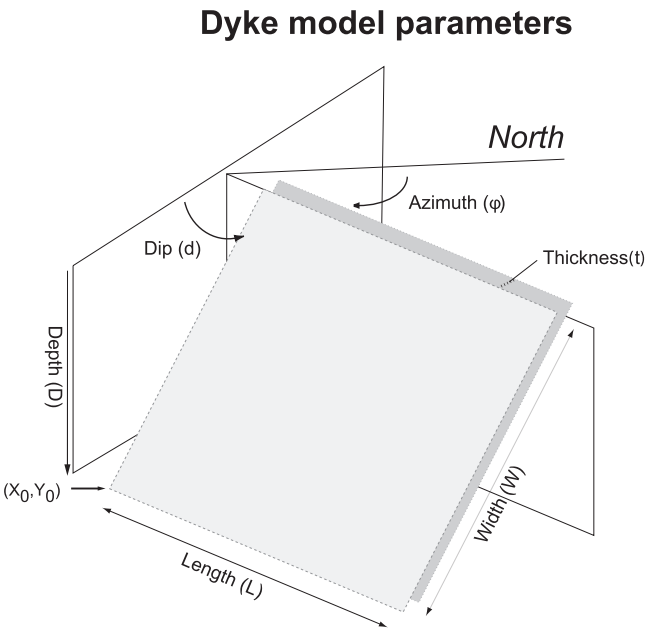

Figure 5. Source model parameters used to compute the 3-D gravity effect produced by a dyke intrusion using the analytical expression by *Okabe* [1979]. Abbreviations are as follows: L and W, length and width of the dyke; d, dip angle of the dyke plane (0° to 90° for a horizontal and vertical dyke respectively); φ, azimuth of the dyke plane (clockwise from the north); t, thickness of the dyke; ρ, density of the material filling the dyke. The arrow denotes the geographical coordinates of the dyke origin (X_0, Y_0) and the depth of the base of the dyke (D).

[24] A similar conclusion can be drawn: taking all the constraints into account, the single source model cannot explain simultaneously the gravity and geodetic observations available for this eruption. Such discrepancies between gravity and geodetic models have already been used to explain intrusive mechanisms on other basaltic volcanoes [*Johnson*, 1992; *Bonforte et al.*, 2007]. As the modeled gravity changes remain too low for acceptable values of the model density and thickness, this leads us to propose that the intrusive dyke is not the only source of the observed gravity changes.

3.2. Dual Source Model

[25] Although the spatial resolution of the gravity network is not very high, the observed gravity signal (Figures 3 and 7) shows signs of two superimposed components: (1) a short-wavelength one, with amplitudes over 75 μGal, correlated with the extension of the eruptive fissures and with the induced ground deformations; and (2) a larger wavelength one, underlined by a roughly WE oriented gravity gradient. This last component suggests a mass increase at depth in the volcanic edifice. The later could be related to the upward migration of the seismic swarm observed prior to the eruption and interpreted by *Aki and Ferrazzini* [2000] as the filling of a reservoir at sea level by one of the lower reservoirs. No significant ground deformation associated with this event was registered by the monitoring networks. Nevertheless, using Radarsat satellite data, *Sigmundsson et al.* [1999] argued that a preeruptive inflation occurred in the few months before the beginning of the eruption. A decrease in range of about 5 cm between the ground surface and the satellite was observed on a 96-day interferogram (2 December 1997 to 8 March 1998). It was interpreted as a volume increase at 2500-m depth beneath the central cone (i.e., close to sea level). The timing of these observations is very similar to the period spanned by our microgravity observations (late November 1997 to early March 1998). The agreement between gravity, seismic and

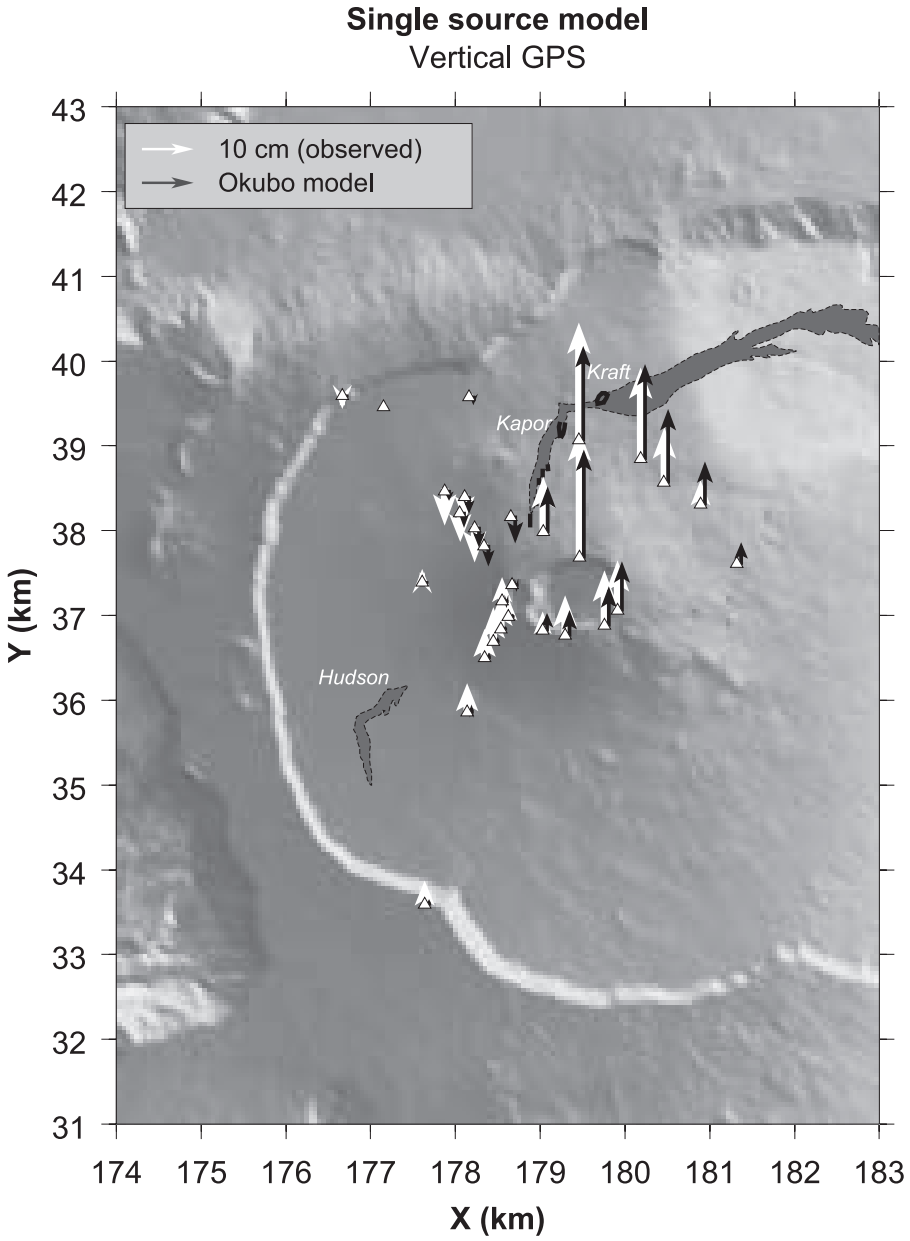

Figure 6. Map of observed and modeled GPS vertical displacement vectors for November 1997 to March 1998. The modeled vectors correspond to our best fit solution (RMS error 3 cm) obtained from the simultaneous inversion of GPS vertical component and gravity data using the tensile dislocation model [*Okubo*, 1992].

satellite data suggests that a mass increase at depth prior to the 1998 eruption is very plausible.

3.3. Proposed Gravity Model

[26] Following the above inferences, we investigate if a dual-source model accounting for magma supplies at shallow (dyke intrusion) and sea level (magmatic reservoir) depths could explain our gravity data. We use Okabe's formulation, which takes into account a more realistic geometry following the topography surface, to model the gravity effect of the dyke intrusion. We use the dyke geometry and density as described in the previous section for this shallow source (called hereafter source S1).

[27] Little information exists about the depth and geometry of the magmatic reservoir below the volcanic edifice. Following *Lenat and Bachèlery* [1990], it could be composed of a large number of relatively small magma reservoirs filled from depth. We use here a point source model to generate the gravity effect of an increase of mass at depth. According to previous studies [*Lenat and Bachèlery*, 1990; *Cayol*, 1996; *Nercessian et al.*, 1996; *Aki and Ferrazzini*, 2000], this reservoir is roughly centered below the summit cone. This enables us to fix the horizontal position and thus, only the depth of this deeper source (called hereafter source S2) will be estimated.

[28] The resulting 3-D gravity model we proposed to explain the 1998 eruption processes is shown in Figure 8.

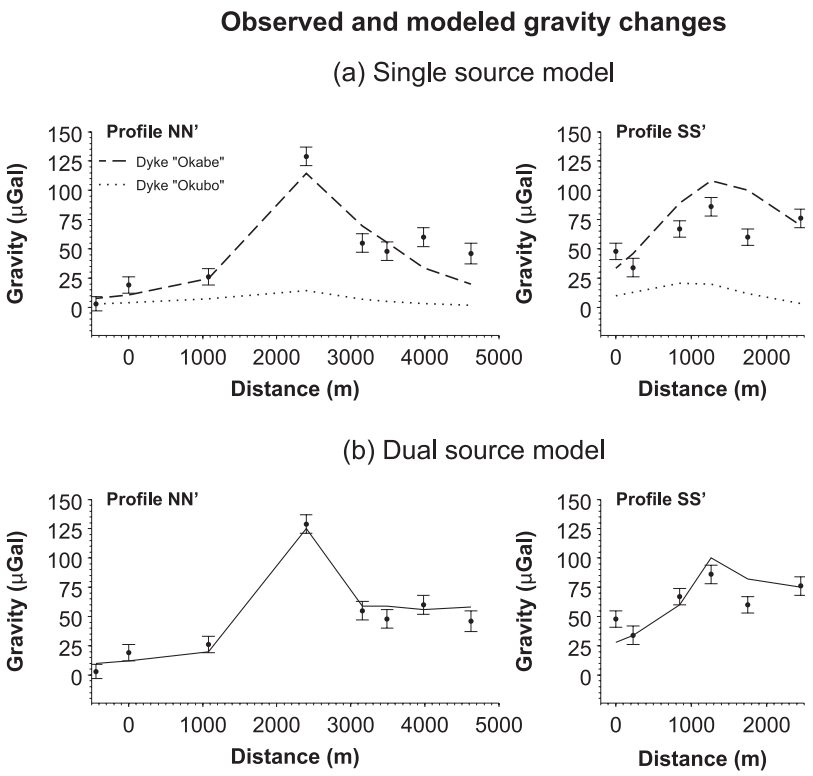

Figure 7. Observed gravity changes between November 1997 and March 1998 along profiles NN′ and SS′ (see location in Figure 3) and computed effects inferred from the inversion of gravity data. (a) Computed effects for the single source model (intrusive dyke). The "Okubo" solution (dotted line) is obtained using the dyke geometry provided by the InSAR and Tilt data and a density of 800 kg.m^{-3} for the intrusive dyke (RMS error 50 μGal). The "Okabe" solution (dashed line) corresponds to the best fit model computed using the meshed dyke model. It corresponds to a mass increase of 3.4 10^{10} kg (RMS error 15 μGal) for the dyke intrusion leading to a minimum dyke thickness of 4 m. (b) Computed effect for the dual source model (solid line) corresponding to the best PPD model shown in Figure 13 (RMS error 10 μGal). The dots with error bars are the observed gravity changes with their standard errors.

It involves four parameters for the intrusive dyke source S1 (length, opening, dip angle and density contrast) and two parameters for the point source S2 (depth and mass increase).

4. Microgravity Data Inversion

4.1. Inversion Method

[29] Using the above defined model, we inverted the observed gravity data to find the source parameters (Table 3). We used a Bayesian formulation, as is commonly used in many geophysical applications, and described, for instance, by *Menke* [1984], *Tarantola* [1987], *Sten and Stoffa* [1996], and *Sambridge* [1999a, 1999b]. In this approach the solution of the inverse problem is described in terms of posterior probability density (PPD) functions that estimate the confidence limits on a given model and provide a full description of the correlation between the model parameters. The calculation of the PPD functions depends only on the observed data, on the a priori constraints of the model parameters and on the statistics of the measurement errors.

[30] To explore the model space, we used an optimized inversion technique based on a genetic algorithm [*Goldberg*, 1989; *Sten and Stoffa*, 1996]. The principles of genetic algorithm (GA) can be found in the work of *Goldberg* [1989] while a detailed description is reported in the work of *Sten and Stoffa* [1996] and *Ying et al.* [2000]. Several applications of GA in geophysical inverse problems are also illustrated by *Sten and Stoffa* [1996], *Beauducel et al.* [2000], *Tiampo et al.* [2000], *Remy et al.* [2003], and *Remy* [2005]. The basic definition of the inversion procedure and its implementation for modeling the gravity data at PDF volcano are given in Appendix A.

4.2. Model Appraisal From a Synthetic Case

[31] We first carried out a synthetic case study in order to evaluate the ability of the proposed model and inversion technique to find a solution reliable from both physical and volcanological points of view. We now focus on (1) the analysis of the sensitivity of our approach to correctly estimate the model parameters and their expected uncertainties and (2) the adjustment of the threshold used in the first stage of inversion process.

[32] The goal here is to replicate as closely as possible actual conditions. So, we chose a synthetic model, similar to that expected for explaining the observed temporal gravity signal. The characteristics of this synthetic model are given in Table 4. Figure 9 shows the computed gravity contribution of each source S1 and S2 separately and their cumu-

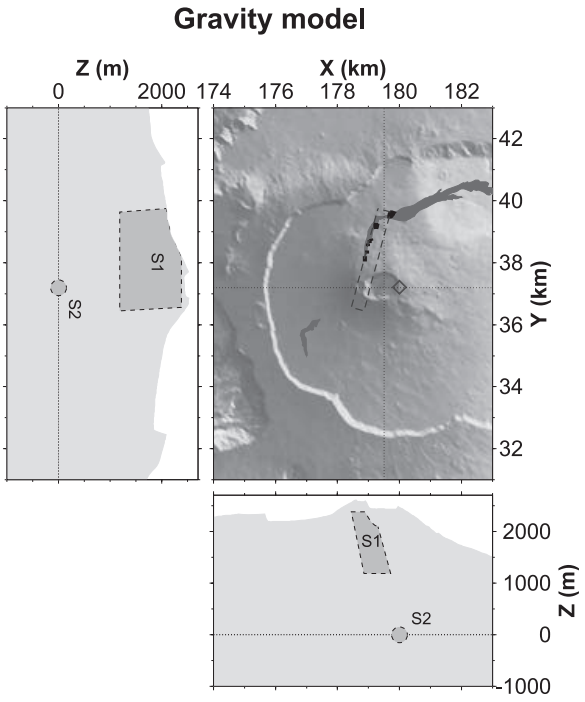

Figure 8. Three-dimensional gravity model proposed for investigating the mass redistributions associated with the March 1998 eruption. The subsurface dyke model (source S1) is defined as shown in Figure 5 with an upper limit adjusted on the topography and on the eruptive fissures (using Okabe formulation). The shallow reservoir is represented as a point source model (source S2) of mass change located below the active cone at variable depths around sea level.

lated effect. As the uncertainty on the temporal gravity changes is 15 μGal, a similar random Gaussian error was added to the theoretical gravity effect calculated at each gravity station for this synthetic model. The mass of the dyke for a given model is computed a posteriori from its inferred parameters and fixed parameters.

[33] The resulting 1-D and 2-D marginal PPD functions, deduced from the gravity inversion, are plotted with the theoretical solutions in Figure 10. They provide meaningful information on the resolution of the model parameters and on their possible correlations. It can be summarized as follows:

4.2.1. Source S1 (Dyke Model)

[34] 1. The mass parameter is well resolved, as indicated by the good fit between the max PPD model and theoretical solution and by the Gaussian shape of the PPD function.

[35] 2. The dyke opening and density parameters are poorly resolved as they can take any value in the range of the width search. They exhibit a strong trade-off as a logical consequence of their relative contribution to the computed mass of a model. For further modeling, we will thus search for the product of these two parameters (t$\Delta\rho$).

[36] 3. The dip parameter is not accurately determined. This is essentially due to the limited number of observations in the vicinity of the eruptive fissures and to the trade-off mentioned above. Typical dip angle values of dyke intrusions in the summit area of the PDF volcano have been estimated from geodetic studies to range within 60° and 70° [*Froger et al.*, 2004; *Fukushima et al.*, 2005]. According to these results and to the dip values given in Table 2, we thus fixed the dip parameter of our model to a mean value of 65°.

4.2.2. Source S2 (Point Source Model)

[37] A trade-off between the depth and the mass parameters is observed for this deeper source. The uncertainties on the temporal gravity changes and the absence of measurement stations in the eastern part of the volcano to constrain the gravity signal over the Grandes Pentes and Grand Brûlé areas, do not enable the inversion process to determine simultaneously these parameters. This also triggers a trade-off between the parameters of source S2 (depth or mass) and the dip angle of source S1 (the deeper the source S2, the higher the angle of the dip for source S1 to explain the observed gravity gradient in the vicinity of the opening fissures). As the depth for source S2 is not well enough constrained by our data, we thus limit the depth range from 700 above to 500 m below the sea level in agreement with the probable location of an upper zone of magma accumulation according to various geophysical data [*Lenat and Bachèlery*, 1990; *Sigmundsson et al.*, 1999; *Peltier et al.*, 2005].

[38] Using the refined theoretical source model, we performed a new synthetic analysis in order to test the ability of the inversion process to determine the three free parameters (L, t$\Delta\rho$, Mass S2). Figure 11 shows the resulting marginal PPD and the 95% confidence intervals determined from the 1-D marginal PPD. It is noteworthy that all inferred parameters now properly fit the initial solution (true model) and lie within narrow confidence intervals, giving us confidence in their estimations. An important conclusion is that, even if it remains a trade-off between the mass increases for sources S1 and S2, the gravity measurements make it possible to quantify both of them at the 95% confidence level with an accuracy of about 2×10^9kg and 10^{10}kg, respectively (see Figure 11).

4.3. Application to the Observed Gravity Data

[39] We applied the retained model and genetic algorithm approach to invert the temporal gravity changes observed

Table 3. Model Parameters Used for the Gravity Data Inversion Using the Genetic Algorithm[a]

Parameters	Fixed Value	Minimum Value	Maximum Value	Step of Search	Bits
		Source S1			
X0, km	179.56	...	...	...	...
Y0, km	36.16	...	...	...	...
D, m	from DEM	...	...	...	...
φ, deg	70	...	...	...	...
W, m	1000	...	...	...	...
L, m	...	2000	5000	10	8
t, m	...	0.5	3	0.2	4
d, deg	...	30	90	1	6
ρ, kg.m^{-3}	...	200	3000	10	5
		Source S2			
Depth, m	...	−5000	1500	12	8
Mass, 10^9kg	...	0	150	0.6	8

[a]See Appendix A and Figures 6 and 8 for model definition and parameterization. The fixed and inferred parameters define the dual source gravity model proposed for the March 1998 eruption, which includes mass changes produced by a dyke intrusion (source S1) and a sea level reservoir (source S2). Depth is given in meters with respect to the sea level.

Table 4. Parameters of the Theoretical Source Gravity Model Used to Perform the Synthetic Tests and the Validation of the Inversion Procedure[a]

Parameter	Value
Source S1	
Length, m	3350
Open, m	2.3
Dip, deg	65
Density, kg.m$-^3$	900
Mass, 10^9 kg	6.93
Source S2	
Depth, m	0
Mass, 10^{10} kg	5.0

[a]Depth is given in meters with respect to the sea level.

between November 1997 and March 1998. Figure 12 displays the resulting 1-D and 2-D marginal PPD functions for this real case. They exhibit quite similar features to those obtained from the synthetic case. The close location of the mean and the maximum PPD models suggests a single peaked distribution meaning that the model parameters are properly estimated. On the base of the observed data and on the proposed model, this data inversion provides a quantification of underground mass changes during the initial phase of the 1998 eruptions. We get values ranged between 3.9 to 8.7 $\times$ 10^9 kg and 4.6 to 7.2 $\times$ 10^{10} kg (95% confidence level) for the dyke intrusion (S1) and for the reservoir at sea level depth (S2), respectively (Table 5).

[40] The model reproduces well the pattern of temporal microgravity observations as illustrated in Figure 7b, which shows the observed and computed gravity changes on the two transects NN′ and SS′. As shown previously in Figure 9, the shorter-wavelength component of the signal is explained by the dyke intrusion, whereas the longer-wavelength component is mainly controlled by the mass increase at depth below the volcanic edifice. Figure 13 displays the observed gravity change, the computed gravity effect for the best model (maximum PPD) and the residual between the observed and modeled gravity signals. The computed signal adequately fits the observed one as shown by the residual amplitudes and by the low RMS value of the adjustment (10 μGal) that remains within the data accuracy.

5. Discussion

[41] In the previous section we showed that the gravity changes observed between November 1997 and March 1998 could have been caused by simultaneous occurrence of two mass increases at different depths. The short-wavelength gravity signal is unambiguously associated with the intrusive dyke whose opening on 9 March 1998 also produced the surface deformations registered by the monitoring networks. Its characteristics have thus been well described by the available geodetic and seismological observations. On the contrary, the source location and geometry of the large wavelength signal is not as well constrained. The timing of this mass increase is not also precisely established but it is likely to have occurred prior to the dyke intrusion within the 4 months preceding the eruption as revealed by our discrete gravity data. This result is in good agreement with the INSAR data covering the same time period which suggest an inflating source at sea level below the volcanic edifice. Even if the source of mass and volume change is not perfectly constrained, both

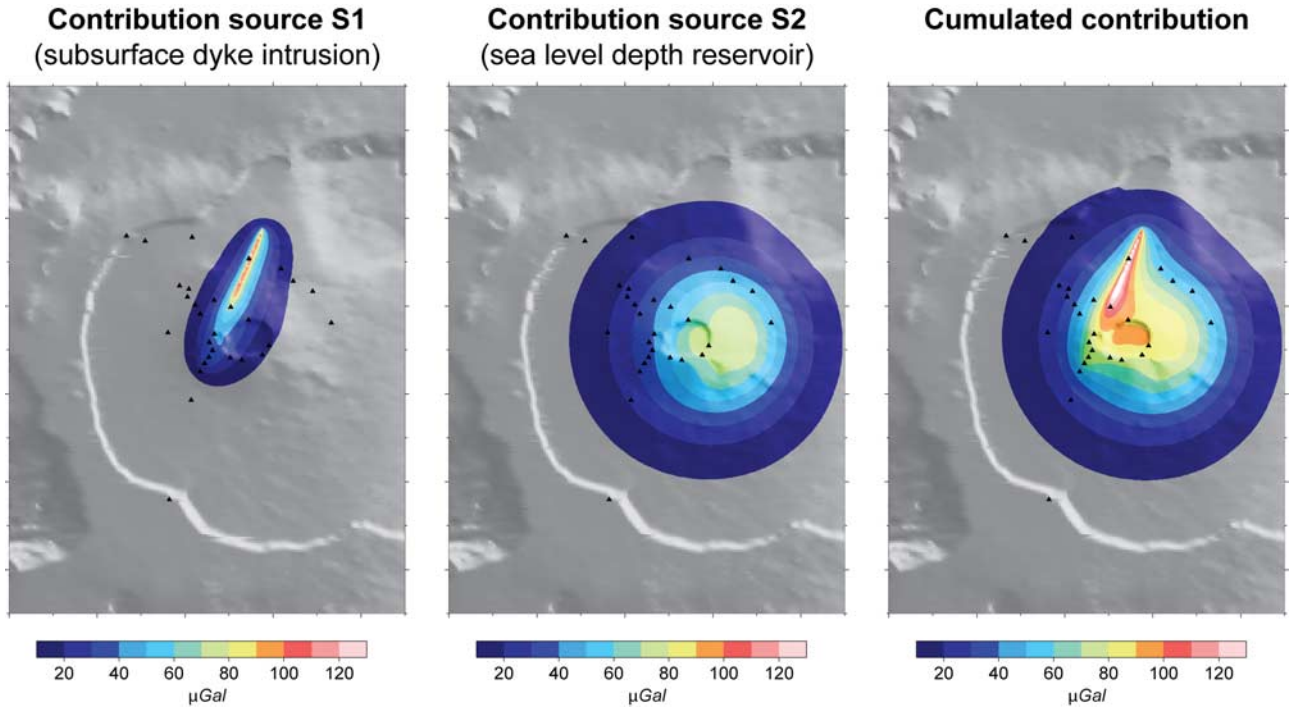

Figure 9. Gravity contributions of the dual source gravity model (in μGal). (left) Contribution for the subsurface source S1 (dyke intrusion). (middle) Contribution for the deeper source S2 (sea level depth reservoir). (right) Cumulated contribution for sources S1 and S2.

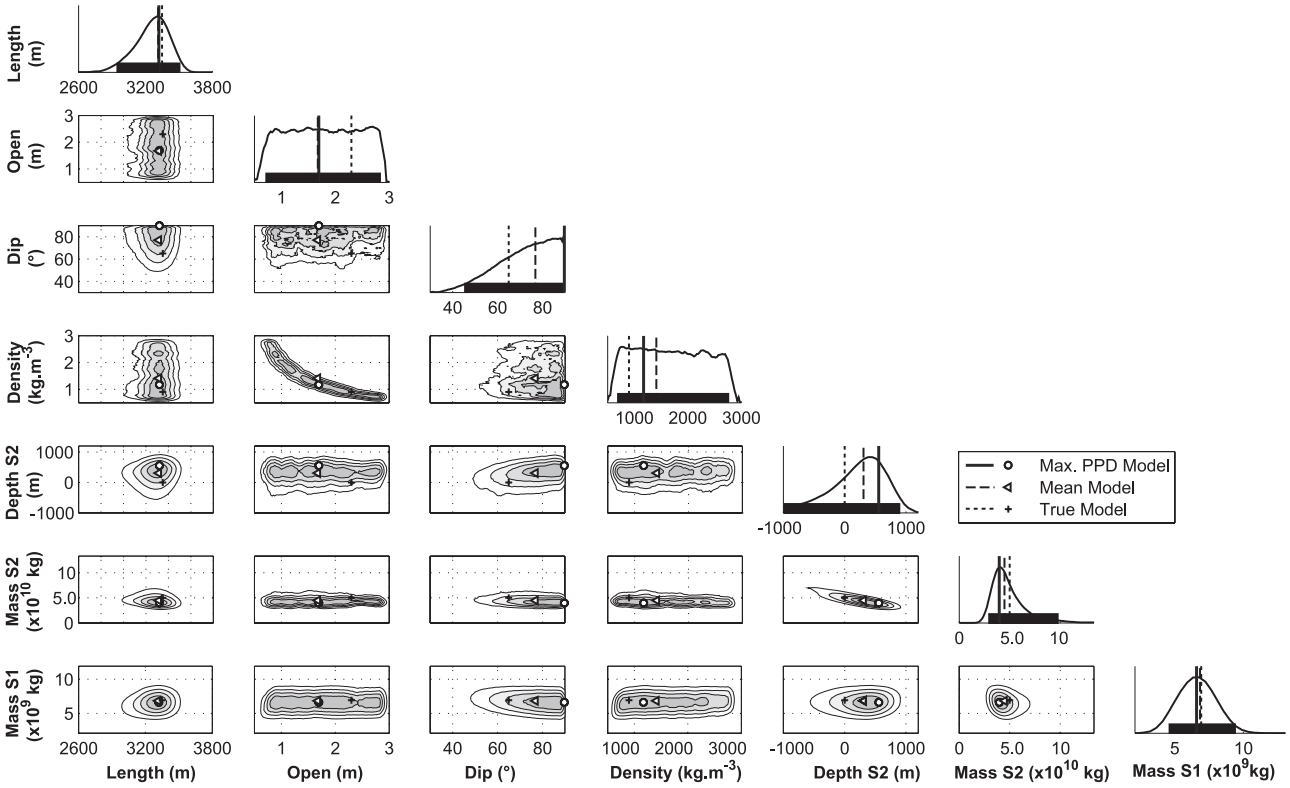

Figure 10. One- and two-dimensional marginal PPD at the 95% confidence level inferred from the inversion of synthetic gravity data using the six parameters model. The maximum PPD and mean models are reported as symbols (dot and triangle) and lines (solid and dashed) for comparison with the true initial model parameters. An error of 15 μGal was added to the synthetic gravity observations. Contour interval is 0.2 times the maximum value. The black thick line indicates in the 1-D plot the 95% confidence interval.

observations suggest the occurrence of a magmatic pulse at depth before the eruption.

[42] Therefore, the results of the present study appear to be consistent with other observations available for this eruption and with the recent hypothesis on magma migration in the plumbing system at PDF volcano. They lead to a quantification of new physical quantities (mass changes) associated with two distinct processes of magma migrations prior and during the March 1998 eruption. We discuss below these quantitative estimations in light of available geological and geophysical information concerning (1) the shallow dyke intrusive processes and (2) the possible magma accumulation in a deeper reservoir below the PDF volcano.

5.1. Constraints on Coeruptive Subsurface Processes (Intrusive Dyke)

[43] As discussed before, the geodetic data available for this eruption (Tilt, InSAR, GPS) are quite well explained using an elastic dislocation model based on rectangular-shaped dyke opening. Accordingly, and considering that our gravity data are not likely to better constrain the dyke geometry, most of these parameters have been set as a priori values in the gravity data inversion. The dyke length being the only free geometrical parameter inferred from the gravity inversion process. In our estimation, this parameter is few hundred of meters longer than the one inferred from the geodetic studies (see Tables 2 and 5). We interpret this larger value as a possible contribution of mass increase related with the magma intrusion which produced the isolated eruption at ''Fred Hudson'' crater. This interpretation is consistent with the INSAR data modeling that clearly shows that the proposed dyke model does not satisfactorily explains the observed fringes on the SW part of the volcano [*Sigmundsson et al.*, 1999]. It thus appears that both ground deformation and mass increase have accompanied the dyke intrusion associated with the SW eruption of 11 March (''Fred Hudson'' crater) as observed for the main eruption initiated three days before. However, the available gravity data do not allow us to better constrain and discriminate the contribution of each process. The mass increase inferred from the data inversion for the dyke model probably involves their cumulated effects.

[44] We estimate the mass increase related to the dyke intrusion to be within 3.9 and 8.7 $\times$ 10^9 kg at the 95% confidence level (Table 5). As our observations are based on discrete measurements spanning 4 months, we cannot discriminate the timing of the intrusive processes that led to such mass increase. We specify that these estimations should be considered as the result of composite processes related with the ascent of fresh magma into the volcanic structure. Induced processes may have complex origins such as mechanical (dilatation-compression of the medium), thermal (cooling of the ascending materials), or hydrothermal

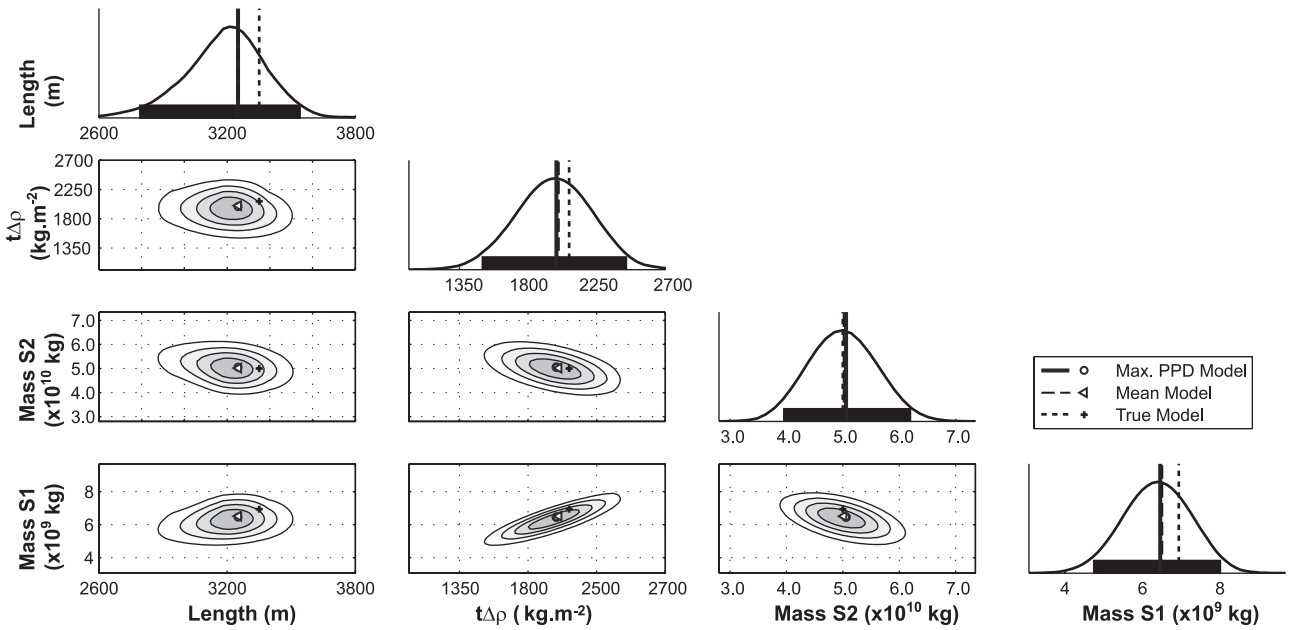

Figure 11. One- and two-dimensional marginal PPD at the 95% confidence level inferred from the inversion of synthetic gravity data using the three parameters model. Same as in Figure 10.

(steam condensation within the shallow hydrothermal system), that will depend on the physical, chemical and mechanical properties of both ascending magma and host medium.

5.2. Constraints on Preeruptive Magma Accumulation (Deep Reservoir)

[45] On the base of the preeruptive uplift signal detected by InSAR data, *Sigmundsson et al.* [1999] estimated to 2×10^6 m^3 the volume of magma accumulated at depth during the 96 days preceding the 9 March 1998 eruption. It is stressed that, whatever the density difference between the fresh magma and the host rock is, the corresponding computed mass increase for this reservoir remains much lower (at least a factor 10) than our estimations inferred from the inversion of discrete gravity data (mass increase of 4.6 to 7.2 $\times$ 10^{10} kg for a source located at sea level depth). The inversion process also indicates that no solution is found for depth values of source S2, 700 m above and below 1400 m respectively to the sea level [*Remy*, 2005]. Assuming the source S2 is located higher within the edifice (700 m a.s.l. for instance), the 95% confidence level estimation of mass changes from 2.9 to 4.6 $\times$ 10^{10} kg, which still remains much higher than the one deduced from the volume change quantified by *Sigmundsson et al.* [1999].

[46] We have also checked if such important mass increase at depth was compatible with the continuous gravity measurements recorded on the sites RER and OVPF stations (see location in Figure 1). Simple computations using a point source model and the parameters given for source S2 (Table 5) indicate that the differential signal produced between those two stations would be too small to be detected, according to the estimated accuracy of the differential gravity (15 μGal). As mentioned before, no significant gravity variations have been detected on these remote stations over periods of a few days preceding the eruption. So, even if no more information can be derived from these continuous data (owing to the duration of the time series and the assumptions made on the instrumental drifts), they do not discard the hypothesis of consequent mass increase at sea level below the edifice during preeruptive stages.

[47] Thus, even though both gravity and InSAR observations indicate a preeruptive magma accumulation at depth below the edifice, there is a significantly difference in the volume and mass changes estimated by each technique. We investigate hereafter possible causes of such discrepancies.

5.3. Causes of Discrepancies Between Geodetic and Gravity Models

[48] We interpret the large wavelength component of the gravity signal measured between November 1997 and March 1998 only in terms of a mass increase at depth below the active cone. Obviously, we cannot exclude that other processes occurring within the volcanic structure may have contributed to induce temporal variations of the gravity field with comparable wavelengths during the same period. One possible cause is a change in the water level of the hydrothermal system of PDF volcano. Such variations were previously pointed out at PDF from microgravity data between 1995 and 1997, during a rest period of the volcano [*Bonvalot et al.*, 2004; *Remy*, 2005]. We cannot discard the hypothesis that the reactivation of the volcano and the upward migration of magma to the surface might have produced perturbations in the hydrothermal system and generated gravity changes during the early stage of the eruption. Unfortunately, we do not have any available observations on the hydrothermal processes during this period to quantify their contribution. Another possible contribution of mass increase might be induced by an E-W compression of the upper volcanic structure in the deforming area. It has been shown from the geodetic data that the dyke opening gradually deformed the edifice from the fissures on the eastern side of the summit cone. The contribution of the dilatation field is estimated through the

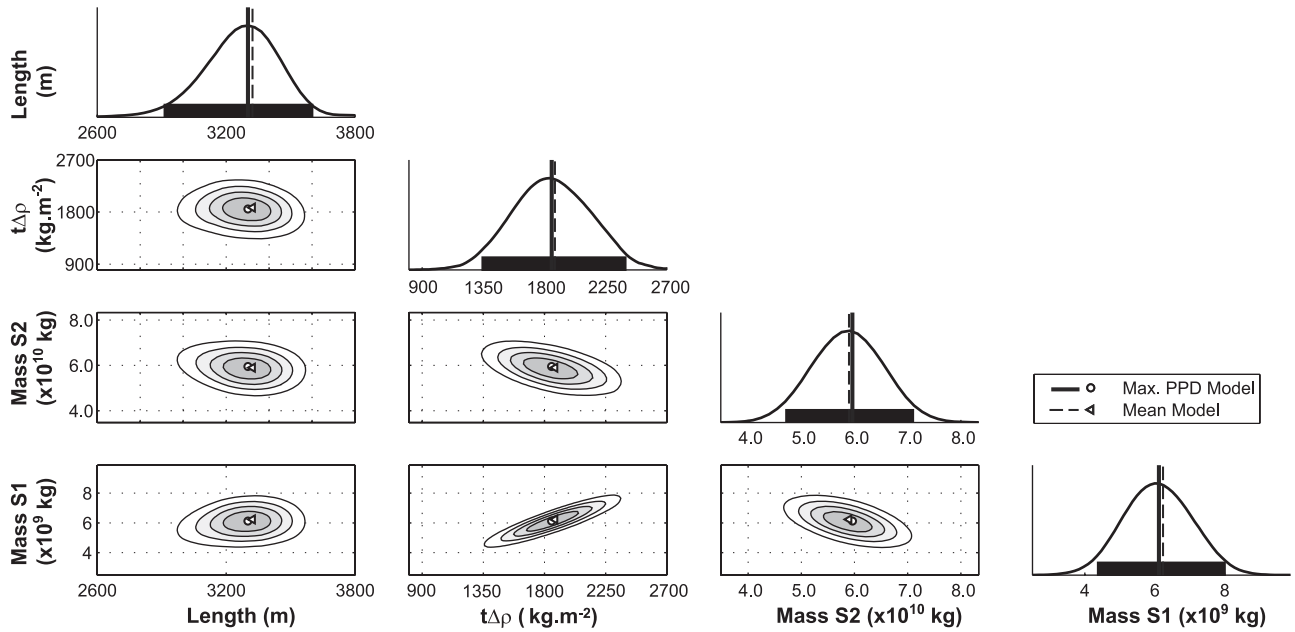

Figure 12. One- and two-dimensional marginal PPD at the 95% confidence level inferred from the inversion of the observed gravity data using the three parameters model. Same as in Figure 10.

Okubo modeling to account for 3–12% of the total gravity change depending on the Poisson ratio and the density of the host rock. These values agree with other estimates inferred from numerical modeling [*Gaillet*, 2006]. Accordingly, our estimation of the mass increase at depth should be thus considered as a maximum value.

[49] As for the microgravity data, some uncertainties can be also expected in the estimation of the volume change inferred from the INSAR data on the base of a Mogi source model (isotropic center of dilatation). Other elastic source models such as sill-like or prolate spheroid would produce a similar amount of vertical displacement but for a bigger volume of magma intrusion than the spherical reservoir [*Fialko et al.*, 2001]. Furthermore, a recent study *Fukushima et al.* [2005] confirmed that the noise variance of SAR interferograms at Piton de la Fournaise volcano is relatively high owing to the importance of tropospheric effects. According to the quantified values of noise variance, the accuracy in the volume estimation for an inflation source is estimated to about $\pm 2 \times 10^6$ m^3 [*Remy*, 2005]. Nevertheless, whatever the type and the geometry of the source may be, it is clear that purely elastic models cannot correctly explain the amplitude of mass increase inferred from the gravity data.

[50] Discrepancies between gravity and deformation data have been already mentioned for other basaltic volcanoes [*Johnson*, 1992; *Johnson et al.*, 2000; *Carbone et al.*, 2003; *de Zeeum-van Dalfsen et al.*, 2004]. To explain such discrepancies, some authors invoked anelastic processes occurring in the magma chamber. We explore this hypothesis using the approach proposed by *Johnson* [1992] for Kilauea and Mauna Loa volcanoes, Hawaii.

5.4. Magmatic Reservoir: Mass Versus Volume Changes

[51] Assuming that ground deformations and gravity changes are explained by a point source model in a homogeneous and elastic medium, *Johnson* [1992] quantifies the relationship between the mass change in a reservoir at depth and the resulting surface deformation as dependant of the mechanical properties of the edifice and magma:

$$\frac{\Delta M}{\Delta V_e} = \frac{\rho}{2(1-\upsilon)} + \frac{2\rho\mu}{3(1-\upsilon)}\left[\frac{1}{K} + \frac{\rho NRT}{P^2\omega}\right], \qquad (3)$$

where ΔM is the magma mass change (kg) within the reservoir, ΔV_e is the edifice volume change (m^3) and ρ is the magma density (kg.m^{-3}). The edifice properties are given by υ, the Poisson's ratio and μ the crustal shear modulus (GPa). The magma properties are given by the terms in brackets representing the free magma compressibility

Table 5. Resulting Model Parameters Inferred From the Inversion of the Temporal Gravity Data Acquired Between November 1997 and March 1998 on the Basis of a Dual Source Model[a]

	Source S1			Source S2: Mass, 10^{10} kg		
	Length, m	t.$\Delta\rho$, kg.m^{-2}	Mass, 10^9 kg	+700 m	0 m	−500 m
Maximum PPD model	3301	1845	6.1	3.7	6.0	7.8
Mean model	3322	1872	6.2	3.7	5.9	7.8
Minimum (IC 95%)	2909	1332	3.9	2.9	4.6	6.4
Maximum (IC 95%)	3606	2403	8.7	4.6	7.2	9.1

[a]Sources S1 and S2 as defined in Figure 8. The RMS of the adjustment between observed and modeled data is 10 μGal. The solutions correspond to the maximum PPD model, mean model, and to the minimum and maximum models within the 95% confidence level. The inferred mass value for source S2 is given for three different depths of source (+700, 0, and −500 m with respect to sea level).

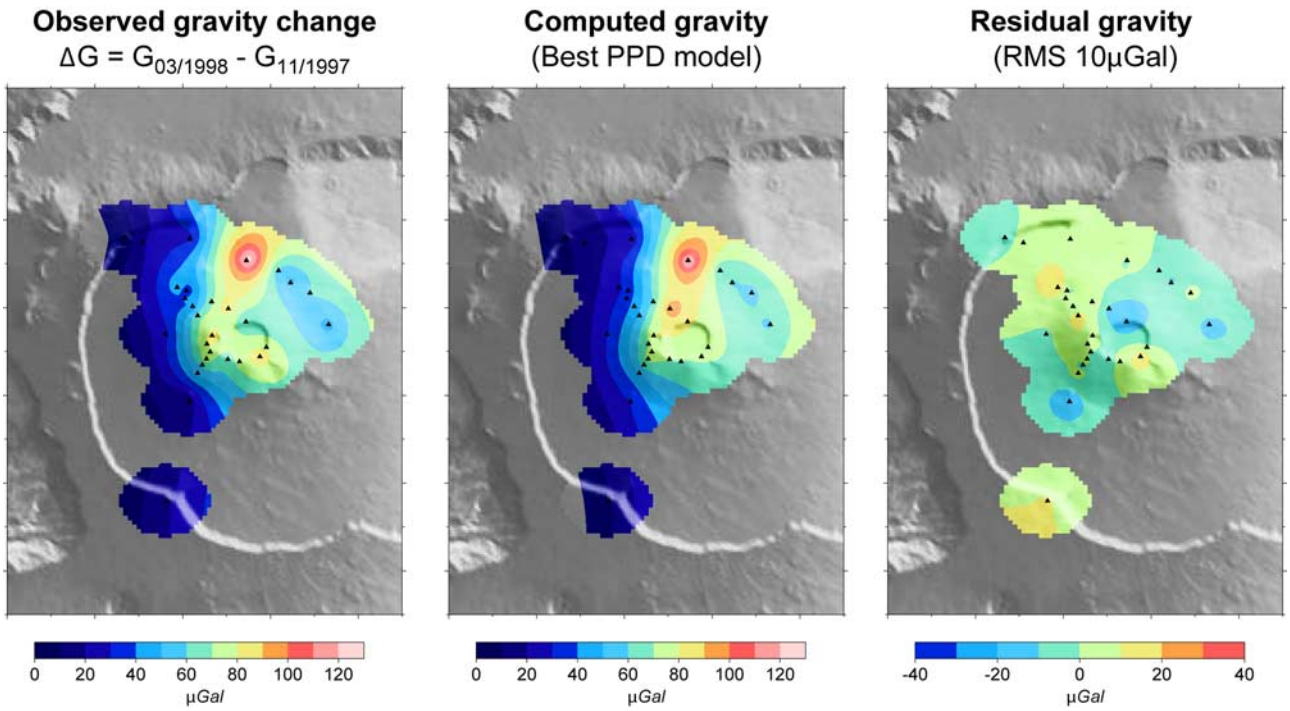

Figure 13. (left) Temporal gravity changes measured between November 1997 and March 1998. (middle) Computed gravity changes for the best PPD model inferred from the gravity data inversion. (right) Residual gravity changes between observed and modeled data (RMS = 10 μGal). Note that a different color scale is used here in order to better contrast the residual gravity map.

$(1/K)$ and the CO_2 gas phase compressibility where K is the magma bulk modulus (GPa), N the CO_2 content of the magma (expressed as total mass fraction), R the gas constant (8.314 $m^3.Pa.mol^{-1}.K^{-1}$), T the reservoir magma temperature (K), P the pressure within the reservoir (MPa) and ω is the mass of one mole of CO_2 (0.044 kg).

[52] Equation (13) shows that for a given $\Delta M/\Delta V_e$ ratio, a relatively strong edifice (high shear modulus μ) will imply a higher compressibility of magma (low K value) and higher gas contents within the reservoir. In other words, the resulting edifice volume change ΔVe induced by magma supply/withdrawn (characterized here by a mass change ΔM) will be accommodated by the amount of contraction-dilatation of the reservoir. Furthermore, it shows that since the bulk modulus of a gas is proportional to pressure, the same amount of CO_2 in a shallower reservoir allows a larger volume of new magma to be accommodated than would be at greater depth.

[53] We used this equation to estimate the CO_2 weight fraction that would be required in an upper magmatic reservoir to explain the gravity and geodetic observations at PDF volcano. The $\Delta M/\Delta Ve$ ratio is computed for the lower and upper values of mass increase of source S2 inferred from our microgravity data inversion. The volume change of the Mogi source given by *Sigmundsson et al.* [1999] from InSAR radar data is used to determine the value of the edifice volume change ΔV_e (3×10^6 m^3) according to the relation $\Delta V_{edifice} = 0{,}67 \times \Delta V_{reservoir}$ [*Delanay and Mc Tigue*, 1994; *Rymer et al.*, 1998]. The pressure P inside the reservoir below the active cone is approximated by the lithostatic pressure as ranged from 46 MPa (reservoir at 700 m a.s.l.) to 76 MPa (reservoir at 500 m b.s.l.). As the corresponding values of mass increase ranges from 2.9×10^{10} to 9.1×10^{10} kg, this leads to an estimation of $C0_2$ weight fraction ranging from 0.0031 to 0.032, respectively.

[54] Obviously, these estimates must be used with caution given the uncertainties on the different parameters deduced from the gravity or geodetic data or arbitrary chosen for the elastic parameters. Nevertheless, it can be noted that the concentrations of CO_2 calculated for the minimum values of mass increase fall within the range estimated by *Gerlach and Graeber* [1985] and *Greenland et al.* [1985], who used geochemical data on Kilauea. Conversely, unrealistic values are found for higher values of mass increases (i.e., magma reservoir located at greater depths). This result supports the hypothesis that the source S2 would be more likely located in the shallow part of PDF volcano (up to few hundred of meters above sea level). Even considering that our mass value might be over-estimated, it indicates that a relatively high concentration of CO_2 could be found in resident magmas accumulated in such shallow reservoirs. This interpretation agrees with the results of gas flux measurements carried out during the 1998 eruption by *Bureau et al.* [1998, 1999] who suggested that large quantities of volatiles (including CO_2) are intercepted at depth before reaching the surface.

[55] Such a high concentration of CO_2 in a shallow reservoir below PDF volcano might explain that a new magma influx could trigger a significant mass increase detectable by surface microgravity data without producing large ground deformation, as observed for Kilauea volcano. It is interesting to observe that a seismic crisis accompanied by surface inflation (tilt changes) and Radon flux increase occurred on 26–27 November 1996. This activity, which

suddenly stopped and did not evolved toward an eruption, was interpreted as an upward migration of magmatic fluids from depths (16 km) to an upper reservoir located at 2.5 km below the summit prior to the 1998 eruption [*GVP*, 1996; *Aki and Ferrazzini*, 2000]. The possibility of a migration of exsolved CO_2 gas from depths into an upper reservoir below the summit might support this hypothesis and explain the unusual high lava fountains observed at the beginning of the March 1998 eruption. We believe that such a physical process that explains the discrepancies between gravity and geodetic data should be considered for further investigations at PDF volcano.

6. Conclusions

[56] Through the analysis of microgravity data acquired at PDF volcano, we quantify the mass redistributions that occurred during the initial stages of the March 1998 eruption and propose a gravity model based on an analytical formulation. Our results provide new constraints on the internal magmatic processes for this eruption and can be summarized as follows:

[57] 1. A gravity increase (amplitude up to 129 μGal) is pointed out within the Enclos Fouqué caldera between November 1997 and March 1998. This temporal gravity signal is dominated by a NNE trending component associated with the ground deformations produced by the dyke intrusion that initiated the 1998 eruption.

[58] 2. The ground deformation data available for this eruption (InSAR, Tilt, GPS) can be explained in terms of a tensile dislocation based on a rectangular shaped dyke opening. Nevertheless, we show that such a model cannot explain both gravity and geodetic data. Thus, we propose a model that takes into account the surface topography in the upper part of the intrusive dyke and added a deeper source of mass change inside the volcano. The proposed gravity model that satisfactorily explains the gravity observations implies mass increases at the subsurface (intrusive dyke) and at greater depth (magma accumulation in a reservoir at sea level depth).

[59] 3. The ascent of magma at sea level depth in the months preceding the 1998 eruption was also proposed from interpretation of satellite InSAR data acquired over the same time interval covered by the gravity data. However, the amplitude of the ground inflation revealed by InSAR data is much smaller than the one expected for the mass increase inferred from our data using an inflating source in a homogeneous elastic half-space. We suggest that this discrepancy indicates high gas content (CO_2) within the reservoir that increases the magma compressibility. This hypothesis, already proposed for Hawaii volcano, could explain the emplacement of large amount of magma at depth without significant surface deformations. An increase of the CO_2 gas content in a shallow reservoir might have been eased by the upward migration of magma observed during the seismic crisis which occurred in 1996.

[60] This study also points out some methodological aspects that should be considered in the future microgravity monitoring at Piton de la Fournaise to improve our understanding of the volcano dynamics. First, the implementation of absolute gravity measurements (in complement to the relative ones) should improve the overall accuracy of the gravity network and of the temporal time series. Second, the implementation of a continuous microgravity monitoring network should greatly contribute to our ability to monitor the time evolution of mass redistributions at PDF and to discriminate their origin (magmatic or hydrothermal). Continuous measurements provided helpful constraints on the dynamics of gravity changes at various volcanoes [*Berrino et al.*, 2000; *Jousset et al.*, 2000; *Branca et al.*, 2003; *Carbone et al.*, 2006]. They are likely to complement other seismic and ground deformation data registered continuously at PDF as well as InSAR time series now available for the most recent eruptions.

[61] The complementarities of microgravity and geodetic techniques are enhanced here, since magma transfers at depth, producing limited deformations at the surface, might be detected through their mass quantification. This study also confirms that only a combination of the information assessed through various monitoring techniques allows us to get the full picture of intrusive mechanisms acting in volcanoes.

Appendix A

A1. Inversion Procedure

[62] Let us define $\mathbf{d}_{\text{obs}}$ the vector of the observed temporal gravity data with their respective errors (vector $\boldsymbol{\sigma}_{\text{obs}}$) and $\mathbf{m}$ the vector of the model parameters:

$$\mathbf{d}_{\text{obs}} = [d_1, d_2, \ldots, d_N]^T; \boldsymbol{\sigma}_{\text{obs}} = [\sigma_1, \sigma_2, \ldots, \sigma_N]^T; \quad \mathbf{m} = [m_1, m_2, \ldots, m_M]^T \tag{A1}$$

where N and M denote the number of gravity observations and number of model parameters respectively and ^{T} denotes the transposed matrix. For a given model $\mathbf{m}$, one can compute the vector $\mathbf{d}_{\text{cal}}$ containing the computed gravity change:

$$\mathbf{d}_{\text{cal}} = \mathrm{g}(\mathbf{m}) = [d_1, d_2, \ldots, d_N]^T. \tag{A2}$$

[63] We used a misfit function to measure the quality of the fit between the observed data $\mathbf{d}_{\text{obs}}$ with errors $\boldsymbol{\sigma}_{\text{obs}}$ and the predicted values $\mathbf{d}_{\text{cal}}$. Assuming a Gaussian distribution of the observed uncertainties, the misfit function for N uncorrelated data is given by:

$$\mathrm{S}(\mathbf{m}) = \frac{1}{2} \sum_{i=1}^{N} \left(\frac{d_{obs}(i) - d_{cal}(i)}{\sigma_{obs}(i)} \right)^2. \tag{A3}$$

[64] It presents a minimum for the best parameters set $\mathbf{m}_{\max}$. The likelihood function or fitness function $\mathrm{L}(\mathbf{m})$ is defined as the a posteriori probability of a model:

$$\mathrm{L}(\mathbf{m}) = \exp(-\mathrm{S}(\mathbf{m})). \tag{A4}$$

This function helps to define the best parameters set $\mathbf{m}_{\max}$ (expected maximum value) and the quality of the function. The posteriori probability density function (PPD) of a gravity model $\mathbf{m}$ for the vector of temporal microgravity observations $\mathbf{d}_{\text{obs}}$ is defined as [*Tarantola*, 1987]:

$$\sigma(\mathbf{m}|\mathbf{d}_{obs}) = \frac{\exp(-S(\mathbf{m}))p(\mathbf{m})}{\int d\mathbf{m} \exp(-S(\mathbf{m}))p(\mathbf{m})}, \tag{A5}$$

where $p(\mathbf{m})$ is the probability density function (PDF) of a model $\mathbf{m}$ independent of the data, $S(\mathbf{m})$ the misfit function defined above, and where the domain of integration spans the entire model space.

A2. Optimization Using Genetic Algorithm

[65] We used an optimized inversion technique based on a genetic algorithm to compute such integrals and explore all regions of the model space. Basically, in the GA technique the model parameters are coded as an unsigned binary string and they are concatenated to form a string called a ''chromosome''. Each chromosome defines a model parameter set $\mathbf{m}$. The search width for each of the model parameters is defined using the a priori information. To start the algorithm, it is necessary to randomly generate an initial model whose parameter values lie within the lower and upper bound of the search width. Then the GA has a relatively simple unfolding based on three following main stages: (1) evaluation of the currently population, (2) selection and (3) crossover/mutation to generate a new population used for the next step of the inversion process. In the selection process, the algorithm will pick the fittest members of the population on the basis of the maximum value given by the fitness function. The maximum value returned by the fitness function will give a maximum of the posteriori probability density (PPD) function for each model parameter. A good knowledge of the PPD function over the whole model space is thus needed to quantify the ability of the inversion technique to find the correct solution and its expected error. As it is difficult to display the PPD in a multidimensional space, several measures of dispersion and marginal density functions are also used to describe the solution. Following *Sten and Stoffa* [1996], the PPD function for a number M of computed models is estimated by:

$$\sigma(\mathbf{m}|\mathbf{d}_{obs}) \cong \frac{\exp(-S(\mathbf{m}))}{\sum\limits_{M} \exp(-S(\mathbf{m}))} \tag{A6}$$

and the marginal PPD of a particular model, the posterior mean model and the posterior model covariance matrix are given respectively by:

$$\sigma(\mathbf{m}_i|\mathbf{d}_{obs}) = \sum_{j,\, j\neq i} \sigma\left(\mathbf{m}_j|\mathbf{d}_{obs}\right) \tag{A7}$$

$$\langle \mathbf{m} \rangle = \sum_{j=1}^{M} \mathbf{m}\sigma(\mathbf{m}|\mathbf{d}_{obs}) \tag{A8}$$

$$C = \sum_{j=1}^{M} (\mathbf{m}_j - \langle \mathbf{m} \rangle)(\mathbf{m}_j - \langle \mathbf{m} \rangle)^{\mathbf{T}} \sigma(\mathbf{m}|\mathbf{d}_{obs}). \tag{A9}$$

The implementation of the genetic algorithm in the microgravity data inversion for PDF volcano was performed through the following steps:

[66] 1. Initial model: As indicated above, our initial gravity model involves six parameters, defined accordingly to the a priori available information and the physical feasibility. Table 3 summarizes the lower and upper bound values and the resolution of the search interval for each parameter. As the gravity data are a well known estimator of mass (one of the best resolved parameter from gravity data inversion), we choose the net mass of the model as the main selection criterion in the inversion process (see below). The mass for each source S1 and S2 was then computed using the corresponding volumetric and density values.

[67] 2. In the first stage several independent runs of GA are made with different starting solutions randomly chosen between the upper and lower bound values of the search width. The main purpose of this first stage is to explore the whole region in the multidimensional model space. Consequently, probability of mutation $P_{m,}$ is fixed to a high value (0.5). The process is stopped when the mean and the variance of the net mass of the gravity model (mass of the dyke and mass increase at depth) do not significantly change, i.e., below an empirically chosen threshold. This stage enables us to estimate the PPD function in its entire domain of definition and makes it possible to detect if the function has numerous peaks with similar fitness values.

[68] 3. In the second stage, the search width is reduced using the 95% intervals determined from the one dimensional marginal PPD computed during the first stage. The purpose of this stage is to evaluate the subset of solutions, which significantly contributes to the sum in equations (A6) and (A7). Consequently, probability of mutation P_m, is fixed to a low value (0.1). As in the previous stage, several independent runs of GA are made but with starting solutions randomly chosen in the reduced search width.

[69] **Acknowledgments.** We thank P. Briole for coordinating the GPS surveys and providing us with the GPS displacements. We thank T. Staudacher, P. Catherine, V. Ferrazzini, J. LeBreton, P. Kowalski, N. Talibart (OVPF, La Réunion), P. Bachelery (Univ. La Réunion), J. Ammann (IPG Paris), G. Juste and C. Luro (IRD Bondy), and M. Larue (IRD La Réunion) for their participation or for logistic help in the gravity field surveys. We thank B. Ducarme (ORB, Bruxelles) for providing us with the tidal parameters. We think also to J-L. Cheminée, who encouraged the implementation of microgravity studies at the PDF volcano, and K. Aki for very constructive discussions on magmatic process at the PDF volcano. Figures were generated with GMT package [*Wessel and Smith*, 1991]. Corrections of English by M. Cumming and M. Jessel were much appreciated. We used for our data inversion the graphical codes provided by Y. Fukushima. The constructive reviews from D. Carbone and P. Jousset have greatly contributed to improve the paper. This study was supported by IPGP (Departement des Observatoires Volcanologiques), IRD (Departement DME) and INSU (programme PNRN). This is IPGP contribution 2317.

References

Abchir, M. A. (1996), Les cendres de Bellecombe: Un événement explosif majeur dans le passé récent du Piton de la Fournaise, Ph.D. thesis, Univ. of Paris VII, Paris.

Aki, K., and V. Ferrazzini (2000), Seismic monitoring and modeling of a volcano for prediction, *J. Geophys. Res.*, *105*, 16,617–16,640.

Bachèlery, P. (1981), Le Piton de la Fournaise (Île de la Réunion): Etude volcanologique structurale et pétrologique, Ph.D. thesis, Univ. de Clermont-Ferrand, Clermont-Ferrand, France.

Barcelo, A. (1996), Analyse des mécanismes hydrologiques en domaine volcanique insulaire à relief jeune. Apports à la connaissance du bilan hydrique. Massif du Piton de la Fournaise (île de la Réunion), Ph.D. thesis, Univ. de Sci. et Technol. du Languedoc, Montpellier, France.

Battaglia, J., and P. Bachèlery (2003), Dynamic dyke propagation deduced from tilt variations preceding the March 9, 1998, eruption of the Piton de la Fournaise volcano, *J. Volcanol. Geotherm. Res.*, *120*, 289–310.

Battaglia, J., K. Aki, and V. Ferrazzini (2005), Location of tremor sources and estimation of lava output using tremor source amplitude on the Piton de la Fournaise volcano: 1. Location of the tremor sources, *J. Volcanol. Geotherm. Res.*, *147*, 268–290.

Beauducel, F., P. Briole, and J. L. Froger (2000), Volcano wide fringes in ERS synthetic aperture radar interferograms of Etna (1992–1999): Deformation or tropospheric effect?, *J. Geophys. Res.*, *105*, 16,391–16,402.

Berrino, G. (2000), Combined gravimetry in the observation of volcanic processes in southern Italy, *J. Geodyn.*, *30*(3), 371–388.

Berrino, G., G. Corrado, R. Magliulo, and U. Riccardi (2000), Continuous gravity record at Mount Vesuvius: A tool to monitor its dynamics, *Phys. Chem. Earth*, *25*(9–11), 713–717.

Bonforte, A., D. Carbone, F. Greco, and M. Palano (2007), Intrusive mechanism of the 2002 NE-rift eruption at Mt Etna (Italy) modelled using GPS and gravity data, *Geophys. J. Int.*, *169*(1), 339–347.

Bonvalot, S., M. Diament, C. Deplus, G. Gabalda, and P. Bachelery (1996), A new microgravity network on Piton de la Fournaise Volcano, paper presented at the Second Workshop on the European Laboratory Volcanoes (EVOP), Int. Assoc. of Volcanol. and Chem. of the Earth's Interior, Santorini, Greece, 2–4 May.

Bonvalot, S., M. Diament, C. Deplus, G. Gabalda, and T. Staudacher (1998a), Microgravity study of Piton de la Fournaise volcano (La Réunion), paper presented at the 23rd European Geophysical Society Meeting, Nice, France, 20–24 April.

Bonvalot, S., M. Diament, and G. Gabalda (1998b), Continuous gravity recording with Scintrex CG-3M meters: A promising tool for monitoring active zones, *Geophys. J. Int.*, *135*, 470–494.

Bonvalot, S., S. Calmant, G. Gabalda, P. Lebellegard, and D. Remy (2003), Activité de l'IRD en gravimétrie et Géodésie, *Rapp. Quadriennal 1999–2002*, 12 pp., Com. Natl. Fr. de Geod. et Geophys., Paris.

Bonvalot, S., D. Remy, C. Deplus, M. Diament, G. Gabalda, J. Amman, T. Catherine, and T. Staudacher (2004), Constraints on subsurface processes on active volcanoes using microgravity monitoring: Results from Piton de la Fournaise (La Réunion), paper presented at IAVCEI General Assembly, Int. Assoc. of Volcanol. and Chem. of the Earth's Interior, Pucon, Chile, 14–19 Nov.

Branca, S., D. Carbone, and F. Greco (2003), Intrusive mechanism of the 2002 NE-Rift eruption at Mt. Etna (Italy) inferred through continuous microgravity data and volcanological evidences, *Geophys. Res. Lett.*, *30*(20), 2077, doi:10.1029/2003GL018250.

Budetta, G., and D. Carbone (1997), Potential application of the Scintrex CG-3M gravimeter for monitoring volcanic activity: Results of field trials on Mt. Etna, Sicily, *J. Volcanol. Geotherm. Res.*, *76*, 199–214.

Bureau, H., F. Pineau, N. Métrich, M. P. Semet, and M. Javoy (1998), A melt and fluid inclusion study of the gas phase at Piton de la Fournaise volcano (Réunion Island), *Chem. Geol.*, *147*, 115–130.

Bureau, H., N. Métrich, M. P. Semet, and T. Staudacher (1999), Fluid-magma decoupling in a hot-spot volcano, *Geophys. Res. Lett.*, *26*, 3501–3504.

Carbone, D., G. Budetta, and F. Greco (2003), Possible mechanisms of magma redistribution under Mt Etna during the 1994–1999 period detected through microgravity measurements, *Geophys. J. Int.*, *153*(1), 187–200.

Carbone, D., L. Zuccarello, G. Saccorotti, and F. Greco (2006), Analysis of simultaneous gravity and tremor anomalies observed during the 2002–2003 Etna eruption, *Earth Planet. Sci. Lett.*, *245*(3–4), 616–629.

Carbone, D., G. Currenti, and C. Del Negro (2007), Elastic model for the gravity and elevation changes before the 2001 eruption of Etna volcano, *Bull. Volcanol.*, *69*, 553–562.

Cayol, V. (1996), Analyse élastostatique tridimensionnelle du champ de déformations des édifices volcaniques par éléments frontières mixtes, Ph.D. thesis, Univ. of Paris VII, Paris.

Cayol, V., and F. H. Cornet (1998), Three dimensional modeling of the 1983–1984 eruption at Piton de la Fournaise Volcano, Reunion Island, *J. Geophys. Res.*, *103*, 18,025–18,037.

Courtillot, V., J. Besse, D. Vandamme, K. Montigny, K. Jeaeger, J. Capetta, and H. Capetta (1986), Deccan flood basalt at the Cretaceous/Tertiary boundary, *Earth Planet. Sci. Lett.*, *80*, 361–374.

Delanay, P. T., and D. F. Mc Tigue (1994), Volume of magma accumulation or withdrawal estimated from surface uplift of subsidence, with application to the 1960 collapse of Kilauea Volcano, *Bull. Volcanol.*, *56*, 7867–7886.

Delorme, H. (1994), Contribution of the deformation monitoring to the knowledge of eruptive processes at Piton de la Fournaise (in French), Ph.D. thesis, Univ. of Paris VII, Paris.

Deplus, C., S. Bonvalot, G. Gabalda, M. Diament, and P. Bachèlery (1996), Bouguer anomaly map of Piton de la Fournaise volcano constrained by new gravity data, paper presented at the Second Workshop on the European Laboratory Volcanoes (EVOP), Int. Assoc. of Volcanol. and Chem. of the Earth's Interior, Santorini, Greece, 2–4 May.

de Zeeum-van Dalfsen, E., H. Rymer, F. Sigmundsson, and E. Sturkell (2004), Net gravity decrease at Askja volcano, Iceland: Constraints on processes responsible for continuous caldera deflation, 1988–2003, *J. Volcanol. Geotherm. Res.*, *139*, 227–239.

Duccan, R. A., J. Backman, and L. Peterson (1989), Reunion hot spot activity through Tertiary time: Initial results from the Ocean Drilling Program, *J. Volcanol. Geotherm. Res.*, *36*, 193–198.

Evans, B. M., and T. H. Staudacher (2001), In situ measurements of gas discharge across fissure associated with lava flows at Réunion Island, *J. Volcanol. Geotherm. Res.*, *106*, 255–263.

Fialko, Y., M. Simons, and Y. Khazan (2001), Finite source modelling of magmatic unrest in Socorro, New Mexico, and Long Valley, California, *Geophys. J. Int.*, *146*, 191–200.

Folio, J. L. (2001), Distribution de la perméabilité dans le massif du Piton de la Fournaise: Apport à la connaissance du fonctionnement hydrogéologique d'un volcan bouclier, Ph.D. thesis, Univ. de la Réunion, St. Denis, France.

Froger, J.-L., Y. Fukushima, P. Briole, T. Staudacher, T. Souriot, and N. Villeneuve (2004), The deformation field of the August 2003 eruption at Piton de la Fournaise, Reunion Island, mapped by ASAR interferometry, *Geophys. Res. Lett.*, *31*, L14601, doi:10.1029/2004GL020479.

Fukushima, Y., V. Cayol, and P. Durand (2005), Finding realistic dike models from interferometric synthetic aperture radar data: The February 2000 eruption at Piton de la Fournaise, *J. Geophys. Res.*, *110*, B03206, doi:10.1029/2004JB003268.

Gabalda, G., S. Bonvalot, and R. Hipkin (2003), CG3TOOL: An interactive computer program to process Scintrex CG-3/3M gravity data for high-resolution applications, *Comput. Geosci.*, *29*, 155–171.

Gaillet, L. (2006), Modélisation numérique des variations de gravité liées aux intrusions de dykes: Application au volcan du Piton de la Fournaise (Île de la Réunion), report, D. E. A Univ. Blaise Pascal (OPGC), Clermont Ferrand, France.

Gerlach, T. M., and E. J. Graeber (1985), Volatile budget of Kilauea Volcano, *Nature*, *313*, 273–277.

Global Volcanism Program (GVP) (1996), Piton de la Fournaise: November intrusion signaled by radon and geophysical measurements, *Bull. Global Volcanism Program, 12/1996*, *23:02*, Smithsonian Inst., Washington, D. C.

Global Volcanism Program (GVP) (1998a), Piton de la Fournaise: First eruption over 5 years begins 9 March, *Bull. Global Volcanism Program, 02/1998*, *21:12*, Smithsonian Inst., Washington, D. C.

Global Volcanism Program (GVP) (1998b), Piton de la Fournaise: Geophysical portrayal of the March fissure eruptions, *Bull. Global Volcanism Program, 03/1998, 23:03*, Smithsonian Inst., Washington, D. C.

Global Volcanism Program (GVP) (1998c), Piton de la Fournaise: April–June lava flows on Plaine des Osmondes and beyond, *Bull. Global Volcanism Program, 06/1998, 23:06*, Smithsonian Inst., Washington, D. C.

Global Volcanism Program (GVP) (1998d), Piton de la Fournaise. New lava flow traverses 12 km across the E flank, *Bull. Global Volcanism Program, 07/1998, 23:07*, Smithsonian Inst., Washington, D. C.

Global Volcanism Program (GVP) (1998e), Piton de la Fournaise. Activity ends with fissure eruptions outside the caldera, *Bull. Global Volcanism Program, 07/1998, 23:07*, Smithsonian Inst., Washington, D. C.

Goldberg, D. E. (1989), *Genetic Algorithms in Search, Optimization and Machine Learning*, Addison-Wesley, Boston, Mass.

Greenland, L. P., W. I. Rose, and J. B. Stokes (1985), An estimate of gas emission and magmatic gas content from Kilauea volcano, *Geochim. Cosmochin. Acta*, *49*, 125–129.

Johnson, D. J. (1992), Dynamics of magma storage in the summit reservoir of Kilauea Volcano, Hawaii, *J. Geophys. Res.*, *97*, 1820–1827.

Johnson, D. J., F. Sigmundsson, and P. T. Delanay (2000), Comment on "Volume of magma accumulation or withdrawal estimated from surface uplift or subsidence with application to the 1960 of Kilauea volcano" by P. T. Delaney and D. F. McTigue, *Bull. Volcanol.*, *61*, 491–493.

Join, J. L., J. L. Folio, and B. Robineau (2005), Aquifers and groundwater within active shield volcanoes: Evolution of conceptual models in the Piton de la Fournaise volcano, *J. Volcanol. Geotherm. Res.*, *147*, 187–201.

Jousset, P., M. Van Ruymbeke, S. Bonvalot, and M. Diament (1995), Performance of two Scintrex CG3M instruments at the fourth International Comparison of Absolute Gravimeters, *Metrologia*, *32*, 231–244.

Jousset, P., S. Dwipa, F. Beauducel, T. Dusquesnoy, and M. Diament (2000), Temporal gravity at merapi during the 1993–1995 crisis: An insight into the dynamical behaviour of volcanoes, *J. Volcanol. Geotherm. Res.*, *100*, 289–320.

Jousset, P., H. Mori, and H. Okada (2003), Elastic models for the magma intrusion associated with the 2000 eruption of Usu Volcano, Hokkaido, Japan, *J. Volcanol. Geotherm. Res.*, *125*, 81–106.

Lenat, J.-F., and P. Bachèlery (1990), Structure et fonctionnement de la zone centrale du Piton de la Fournaise, in *Le volcanisme de la Réunion: Monographie*, edited by J. F. Lenat, pp. 257–296, Cent. de Rech. Volcano., Obs. Phys. du Globe de Clermont-Ferrand, Univ. Blaise Pascal, Clermont-Ferrand, France.

Menke, W. (1984), *Geophysical Data Analysis: Discrete Inverse Theory*, 260 pp., Elsevier, New York.
Nercessian, A., A. Hirn, J. C. L. Lepine, and M. Sapin (1996), Internal structure of Piton de la Fournaise volcano from seismic wave propagation and earthquake distribution, *J. Volcanol. Geotherm.*, 123–143.
Okabe, M. (1979), Analytical expressions for gravity anomalies dues to homogeneous polyhedral bodies and translations into magnetic anomalies, *Geophysics*, *44*(4), 730–741.
Okada, Y. (1985), Surface deformation due to shear and tensile faults in half space, *Bull. Volcanol. Soc. Am.*, *75*, 1135–1154.
Okada, Y. (1992), Internal deformation due to shear and tensile faults in a half-space, *Bull. Seismol. Soc. Am.*, *82*(2), 1018–1040.
Okubo, S. (1992), Gravity and potential changes due to shear and tensile faults in a half-space, *J. Geophys. Res.*, *97*, 7137–7144.
Okubo, S., and H. Wanatabe (1989), Gravity change caused by fissure eruption, *Geophys. Res. Lett.*, *16*, 445–448.
Peltier, A., V. Ferrazzini, T. Staudacher, and P. Bachèlery (2005), Imaging the dynamics of dyke propagation prior to the 2000–2003 flank eruptions at Piton de La Fournaise, Reunion Island, *Geophys. Res. Lett.*, *32*, L22302, doi:10.1029/2005GL023720.
Remy, D. (2005), Analyse et inversion de séries interférométriques et microgravimétriques temporelles sur les volcans actifs: Apport à la quantification d'effets de sites et à la compréhension de la dynamique volcanique, Ph.D. thesis, Univ. of Paris VII, Paris.
Remy, D., S. Bonvalot, P. Briole, and M. Murakami (2003), Accurate measurement of tropospheric effects in volcanic area from SAR interferometry data: Application to Sakurajima volcano (Japan), *Earth Planet. Sci. Lett.*, *213*(3–4), 299–310.
Rousset, D., A. Lesquer, A. Bonneville, and J.-F. Lenat (1989), Complete gravity study of Piton de la Fournaise volcano, Réunion Island, *J. Volcanol. Geotherm. Res.*, *36*, 37–52.
Rymer, H. (1994), Microgravity change as a precursor to volcanic activity, *J. Volcanol. Geotherm. Res.*, *100*, 289–320.
Rymer, H., J. Cassidy, C. Locke, and F. Sigmundsson (1998), Post-eruptive gravity changes from 1990 to 1996 at Krafla volcano, Iceland, *J. Volcanol. Geotherm. Res.*, *87*, 141–149.
Sambridge, M. (1999a), Geophysical inversion with a neighbourhood algorithm—II. Searching a parameter space, *Geophys. J. Int.*, *138*, 479–494.
Sambridge, M. (1999b), Geophysical inversion with a neighbourhood algorithm—I. Appraising the ensemble, *Geophys. J. Int.*, *138*, 727–746.
Seigel, H. O., I. Brcic, and P. Mistry (1993), *A Guide to High Precision Land Gravimeter Surveys*, in Scintrex Ltd., Concord, Ont., Canada.
Sigmundsson, F., P. Durand, and D. Massonnet (1999), Opening of an eruptive fissure and seaward displacement at Piton de la Fournaise volcano measured by RADARSAT satellite radar interferometry, *Geophys. Res. Lett.*, *26*, 533–536.
Sten, M. K., and P. L. Stoffa (1996), Bayesian inference, Gibbs' sampler and uncertainty estimation in geophysical inversion, *Geophys. Prospect.*, *44*, 313–350.
Tarantola, A. (1987), *Inverse Problem Theory Methods for Data Fitting and Model Parameters Estimation*, 615 pp., Elsevier, Amsterdam.
Tiampo, K. F., J. B. Rundle, J. Fernandez, and J. O. Langbein (2000), Spherical and ellipsoidal volcanic sources at Long Valley caldera, using a genetic algorithm inversion technique, *J. Volcanol. Geotherm. Res.*, *102*, 189–206.
Torge, W. (1989), *Gravimetry*, Walter de Gruyter, Berlin.
Villari, L. (1969), Sulla densità delle vulcaniti, *Riv. Mineria Sicilina*, *112*, 1–4.
Violette, S. (1993), Modélisation des circulations d'eau dans le volcan de la Fournaise: Approche du bilan hydrologique et des échanges thermiques, Ph.D. thesis, Univ. of Paris VI, Paris.
Wessel, P., and W. H. F. Smith (1991), Free software helps map and display data, *Eos Trans., AGU*, *72*, 441.
William, H., and A. McBirney (1979), *Volcanology*, W. H. Freeman, San Francisco, Calif.
William-Jones, G., and H. Rymer (2002), Detecting volcanic eruption precursors: A new method using gravity and deformation measurements, *J. Volcanol. Geotherm. Res.*, *113*, 379–389.
Ying, J., S. Suingh, and B. Hornby (2000), Sensitivity study using genetic algorithm: Inversion of amplitude variations with slowness, *Lithos Sci. Rep.*, *2*, 35–49.

S. Bonvalot, G. Gabalda, and D. Remy, Institut de Recherche pour le Développement, LMTG (Université de Toulouse-CNRS-IRD-OMP), 14 av. E. Belin, F-31400 Toulouse, France. (bonvalot@ird.fr)
C. Deplus and M. Diament, Institut de Physique du Globe de Paris, CNRS, 4 Place Jussieu, Case 89, F-75252 Paris Cedex 05, France.